

# The Role of Dwarf Galaxy Interactions in Shaping the Magellanic System and Implications for Magellanic Irregulars

Gurtina Besla<sup>1,2\*</sup>, Nitya Kallivayalil<sup>3</sup>, Lars Hernquist<sup>2</sup>, Roeland P. van der Marel<sup>4</sup>, T.J. Cox<sup>5</sup>, and Dušan Kereš<sup>6</sup>

*Department of Astronomy & Astrophysics, Columbia University, 550 West 120th Street, New York, NY 10027, USA*

*Harvard-Smithsonian Center for Astrophysics, 60 Garden Street, Cambridge, MA 02138*

*Department of Astronomy, Yale University, New Haven, CT 06520, USA*

*Space Telescope Science Institute, 3700 San Martin Drive, Baltimore, MD 21218*

*Carnegie Observatories, 813 Santa Barbara Street, Pasadena, CA 91101, USA*

*Department of Astronomy and Theoretical Astrophysics Center, University of California, Berkeley, CA 94720-3411, USA*

9 January 2012

## ABSTRACT

We present a novel pair of numerical models of the interaction history between the Large and Small Magellanic Clouds (LMC and SMC, respectively) and our Milky Way (MW) in light of recent high precision proper motions from the Hubble Space Telescope (Kallivayalil et al. 2006a,b). These proper motions imply that the Magellanic Clouds (MCs) are moving  $\sim 80$  km/s faster than previously considered. Given these velocities, cosmological simulations of hierarchical structure formation favor a scenario where the MCs are currently on their first infall towards our Galaxy (Besla et al. 2007; Boylan-Kolchin et al. 2011; Busha et al. 2011). We illustrate here that the observed irregular morphology and internal kinematics of the Magellanic System (in gas and stars) are naturally explained by interactions between the LMC and SMC, rather than gravitational interactions with the MW. These conclusions provide further support that the MCs are completing their first infall to our system. In particular, we demonstrate that the Magellanic Stream, a band of HI gas trailing behind the Clouds 150 degrees across the sky, can be accounted for by the action of LMC tides on the SMC before the system was accreted by the MW. We further demonstrate that the off-center, warped stellar bar of the LMC and its one-armed spiral, can be naturally explained by a recent direct collision with its lower mass companion, the SMC. Such structures are key morphological characteristics of a class of galaxies referred to as Magellanic Irregulars (de Vaucouleurs & Freeman 1972), the majority of which are not associated with massive spiral galaxies. We infer that dwarf-dwarf galaxy interactions are important drivers for the morphological evolution of Magellanic Irregulars and can dramatically affect the efficiency of baryon removal from dwarf galaxies via the formation of extended tidal bridges and tails. Such interactions are important not only for the evolution of dwarf galaxies but also have direct consequences for the buildup of baryons in our own MW, as LMC-mass systems are believed to be the dominant building blocks of MW-type halos.

**Key words:** galaxies: interactions — galaxies: kinematics and dynamics — galaxies: evolution — galaxies: irregular — Magellanic Clouds

## 1 INTRODUCTION

The Large Magellanic Cloud (LMC) is the prototype for a class of dwarf galaxies known as Magellanic Irregulars. Like the LMC, these galaxies are characterized by being gas rich, one-armed spirals with off-center bars

\* Hubble Fellow e-mail: gbesla@astro.columbia.edu

(de Vaucouleurs & Freeman 1972). Although there are numerous examples of Magellanic Irregulars in our Local Volume, they are rarely found about massive spirals. This has been confirmed by recent studies of the frequency of LMC analogs about Milky Way (MW) type galaxies in the SDSS DR7 catalog (Liu et al. 2011; Tollerud et al. 2011). Based on similar statistics, de Vaucouleurs & Freeman (1972) concluded that the LMC has necessarily experienced little or no distortion due to interactions with the MW, and so its characteristic asymmetric features must owe to some other process.

The idea that the LMC’s evolution has not been dictated by interactions with the MW is given further credence by the distance morphology relationship exhibited by MW and M31 satellites, whereby gas rich satellites are located at larger galactocentric radii than gas poor spheroidals. The Magellanic Clouds (MCs), at a mere 50–60 kpc away, are notable exceptions to this relationship, leading van den Bergh (2006) to describe them as interlopers in our system. Along the same lines, recent studies indicate that the LMC is much bluer in color relative to analogs in its magnitude range (Tollerud et al. 2011; James & Ivory 2011). This fact is difficult to reconcile with the expected gas loss and quenching of star formation the LMC should have incurred if it were indeed a long-term companion of the MW (Grcevich & Putman 2009). These conclusions are further supported by recent proper motion measurements (Kallivayalil et al. 2006a,b), which indicate that the LMC is moving  $\sim 80$  km/s faster than previously believed (Gardiner & Noguchi 1996). Given the measured energetics of the LMC’s orbit today, backward orbital integration schemes (Besla et al. 2007) and statistics from large scale cosmological simulations (Boylan-Kolchin et al. 2011; Busha et al. 2011) indicate that the LMC is likely on its first infall towards the MW. Consequently, the MW cannot have been the driver of its morphological evolution.

In this study we ask the following: if not interactions with the MW, then what is the origin of the asymmetric appearance of the LMC and what is its connection to Magellanic Irregulars in general?

Notably, the LMC has a nearby companion, the Small Magellanic Cloud (SMC). In fact, many Magellanic Irregulars also have companions (Odehahn 1994), although the frequency of such configurations is debated (Wilcots 2009). Particularly striking examples include the Magellanic Irregular galaxies NGC 4027 (Phookun et al. 1992) and NGC 3664 (Wilcots & Prescott 2004); both have a low mass companion to which each is connected by a bridge of gas. The LMC and SMC are also connected by a bridge of HI gas, known as the Magellanic Bridge (Kerr 1957), suggesting that interactions between dwarf pairs may hold clues to understanding the current morphology of Magellanic Irregular galaxies.

In addition to the Magellanic Bridge, the MCs are associated with both leading and trailing streams of gas, referred to as the Leading Arm and Magellanic Stream, respectively. The Magellanic Stream extends over 150 degrees across the southern sky (Nidever et al. 2010, 2008; Putman et al. 2003; Wannier & Wrixon 1972; Mathewson et al. 1974) and has been traditionally modeled as the product of MW tides (Murai & Fujimoto 1980; Heller & Rohlfs 1994; Lin et al. 1995; Gardiner et al.

1994; Gardiner & Noguchi 1996; Bekki & Chiba 2005; Connors et al. 2005; Mastropietro et al. 2005; Ružička et al. 2009, 2010) and ram pressure stripping (Mastropietro et al. 2005; Moore & Davis 1994). A purely hydrodynamic solution cannot pull material forward to explain the Leading Arm Feature, meaning that MW tides must be invoked in some form in all of these models. However, on a first infall, MW tides are negligible until very recently; it is thus difficult to reconcile the new proper motions and updated orbits with the formation of the Magellanic Stream, Bridge and Leading Arm in the context of the existing scenarios.

Alternatively, Besla et al. (2010) (hereafter B10) introduced a model to explain the observed large scale gas morphology of the Magellanic System through tidal interactions between the LMC and SMC (see also, Diaz & Bekki 2011a). Because MW tides are not responsible for removing material from the system, this picture is consistent with a first infall scenario. In this model, the Magellanic Bridge, Arm and Stream are hypothesized to be analogs of the classical Toomre & Toomre (1972) tidal bridge and tail scenario and should be commonly found about interacting pairs/groups of dwarf galaxies.

Here we explore whether interactions between the MCs can also account for the internal morphology and kinematics of the LMC and therefore shed light on the dynamical state of Magellanic Irregulars more generally.

In particular, the nature of the LMC’s off-centered stellar bar has been a long standing puzzle, as it is not present in any other tracer of the interstellar medium (ISM); it is neither apparent in the HI gas disk nor a site of active star formation as traced by H $\alpha$  emission. Strong bars in more massive galaxies serve to funnel gas towards the center; streaming motions and characteristic “S-shaped” isovelocity contours are thus evident in their gas velocity fields. While weak large scale streaming motions along the bar may be evident in the LMC HI velocity field (Kim et al. 1998), the expected “S-shaped” isovelocity contours are not present.<sup>1</sup> Interestingly, this is also true of many other Magellanic Irregulars (Wilcots 2009): bars in these systems do not appear to strongly affect the underlying gas distribution. There is also evidence that the bar may be warped relative to the LMC disk plane (Subramaniam 2003; Lah et al. 2005; Koerwer 2009). Using relative distance measurements to Cepheids, Nikolaev et al. (2004) concluded that the bar is in fact located  $\sim 0.5$  kpc in front of the main disk. For this reason it has been described as a “levitating” bar. Zaritsky (2004) suggests that this may be a result of viewing a tri-axial stellar bulge that is embedded in a highly obscuring thick disk. Along the same lines, Zhao & Evans (2000) postulate that the off-centered bar is an unvirialized structure, inclined relative to the plane of the LMC disk by as much as 25 degrees in order to explain the microlensing optical depth observed towards the LMC. Clearly, the nature of the LMC’s bar is an ongoing subject of debate.

We posit here that a recent direct collision between the LMC and SMC has left the LMC with a warped, off-

<sup>1</sup> Kim et al. (1998) comment on the existence of a distorted S-shaped isovelocity contour across the LMC’s minor axis. However, Olsen & Massey (2007) find that this feature straightens out when the higher proper motions are accounted for.

centered stellar bar and pronounced one-armed spiral. We further claim that such asymmetric structures are characteristic of Magellanic type galaxies undergoing minor mergers. In this study we illustrate that such a scenario is consistent with a first infall towards our MW and can simultaneously explain both the morphology and kinematics of the LMC as well as the large scale gas morphology of the Magellanic System. Thus, Magellanic Irregulars with nearby companions should also be associated with faint extended gaseous tails and bridges. As in the Magellanic System, such features could hold  $\sim 50\%$  of the baryonic mass of the original system, indicating that dwarf-dwarf tidal interactions are an important mechanism for the loss of baryons in low mass systems (see also, D’Onghia et al. 2009), as a consequence of resonant interactions between spinning disks (D’Onghia et al. 2010).

We stress that the goal of our study here is not to reproduce every detail of the Magellanic System, as we have not conducted a complete parameter search of all the possible orbital configurations, mass ratios and gas fractions, which influence the final outcome. The aim of this investigation is rather to determine which of the observed peculiarities of the Magellanic System can be directly linked to interactions between the MCs.

Moreover, our work has broader implications for understanding the properties of accreted satellites. Minor mergers are frequent events that shape galaxies and their halos; however, little attention has been given to the accretion of binary pairs or groups of smaller galaxies (but see, D’Onghia & Lake 2008; Sales et al. 2007). This study represents a first step towards understanding the morphological evolution and gas loss rates of such galaxies immediately after their capture by a massive host. LMC mass objects are expected to be the primary building blocks of MW type galaxies (Stewart et al. 2008), making this study of direct relevance to our understanding of the evolution of the MW.

In this paper we begin by outlining our methodology and introducing two possible models for the interaction history of the MCs, one of which invokes a recent direct collision between the MCs. In the subsequent sections we discuss the resulting large scale gas structure and internal structure and kinematics of the LMC. The results for the SMC and the expected stellar counterpart to the Magellanic Stream will be presented in future work.

## 2 METHODOLOGY

We follow the general method outlined in B10 to set up the initial galaxy models and orbits in order to reproduce the observed large scale gaseous structure of the Magellanic System. Details about our numerical methods, initial conditions and chosen orbital parameters are described below.

### 2.1 Numerical Methods

All of the numerical simulations performed in this work use the N-body smoothed-particle hydrodynamics (SPH) code, Gadget3 (Springel 2005). The Gadget3 code incorporates a subresolution multiphase model of the ISM that includes radiative cooling (Springel & Hernquist 2003), and incorporates a fully conservative approach to integrating

the equations of motion (Springel & Hernquist 2002). Star formation from the cold phase (i.e. all cold gas - no distinction is made between atomic and molecular components) follows a Schmidt volume density law  $\rho_{\text{SFR}} \propto \rho_{\text{gas}}^N$  (with  $N = 1.5$ ) that is normalized to approximate the star formation rate of the MW. A local threshold volume density cutoff of  $0.004 \text{ M}_{\odot} \text{pc}^{-3}$  is adopted, below which stars do not form. As pointed out by many authors (e.g., Kuhlen et al. 2011; Hopkins et al. 2011; Gnedin & Kravtsov 2010; Robertson & Kravtsov 2008), such a star formation prescription is likely inappropriate for dwarf galaxies. We discuss the implications of our adopted prescriptions to our results in § 6.1.

Stellar feedback in the form of galactic winds is not employed in our simulations; however, we comment on the relative importance of outflows to the formation of the Magellanic Stream in Appendix B.

We note that the reliability of SPH for cosmological simulations has recently been called into question by Vogelsberger et al. (2011); Sijacki et al. (2011); Keres et al. (2011); Torrey et al. (2011); Bauer & Springel (2011). However, comparisons between SPH and calculations done with the moving mesh code Arepo (Springel 2010), show good agreement for applications involving galaxy collisions, at least when the subresolution model mentioned above is used to represent star-forming gas (Hayward et al. 2011, in prep). The tests done by e.g. Sijacki et al. (2011) indicate that SPH can fail when applied to situations in which gas in very different phases are in motion relative to one another. The use of an effective equation of state to describe the ISM effectively circumvents this issue because the different phases of the gas are not modeled explicitly.

### 2.2 Initial Conditions

The initial conditions for the construction of the LMC and SMC galaxies used for all models are outlined in Table 1. As in B10, the total initial mass of the LMC is determined using current halo occupation models to relate the observed stellar mass of the LMC to its original halo mass before infall into the MW halo (Guo et al. 2010). Reflecting their stellar mass ratio, the SMC is then chosen to be 10 times less massive than the LMC. Consequently, the MCs are modeled here to have infall masses an order of magnitude larger than employed in previous models. The number of particles of each component (gas, stars, dark matter) are chosen such that the mass resolution per particle of a given type is roughly the same in both galaxies.

The SMC is modeled with an extended gaseous disk with a scale length 3 times that of the stellar component. Much larger ratios are common for isolated dwarfs found in voids (Kreckel et al. 2011), and neutral hydrogen observations of SMC-like dwarfs with the Westerbork Synthesis Radio Telescope by Swaters et al. (2002) find HI disk scale lengths ranging from 1.4-4.5 kpc (Connors et al. 2005). Our adopted scale length of 3.3 kpc is consistent with the upper end of the observed range.

The LMC is modeled with gas and stellar disks with the same scale length, rather than with an extended gaseous disk. In reality, the interaction with the ambient hot gaseous halo of the MW would serve to truncate the LMC’s extended gas disk. The scale height of the stellar disk is taken as 0.2 of

the disk scale length. The modeled scale height of the LMC's stellar disk is thus initially  $z_0 = 0.34$  kpc (the observed value today is  $R_{\text{disk}} = 1.4$  kpc and  $z_0 = 0.27$  kpc; van der Marel et al. 2002). The gaseous disk height is determined by self-gravity and the pressurization of the ISM, as prescribed by the chosen effective equation of state (Springel et al. 2005).

The dark matter halos of the LMC and SMC follow Hernquist potentials (Hernquist 1990). The scale radius for the Hernquist potential ( $r_H$ ) is related to the scale radius of the corresponding NFW halo ( $r_S = R_{200}/C$ ) (Navarro et al. 1997) as described in Springel et al. (2005):

$$r_H = r_S \sqrt{2 \left( \ln(1+C) - \frac{C}{1+C} \right)}, \quad (1)$$

where  $C$  is the concentration parameter. Values for  $C$ ,  $r_S$  and  $r_H$  are listed in Table 1.

The MW is modeled as a static NFW potential with a total mass of  $1.5 \times 10^{12} M_\odot$ ,  $C = 12$ , virial radius of  $R_{\text{vir}} = 300$  kpc, and  $R_{200} = 220$  kpc (radius where the average density is 200 times the critical density of the Universe). As in B10, dynamical friction from the MW halo is not explicitly accounted for, but is expected to have little impact on the orbit in a first passage (see Besla et al. 2007, Figure 4). Dynamical friction between the MCs, on the other hand, plays a much more important role in their orbital evolution and is captured explicitly by modeling these two galaxies with live dark matter halos.

The resulting rotation curves for the MCs are plotted in Figure 1. The initial SMC rotation curve peaks at  $V_{\text{rot}} = 60$  km/s at 3 kpc from the center, as expected from HI kinematics (Stanimirović et al. 2004); the SMC is initially a well-behaved disk galaxy. The initial simulated LMC rotation curve peaks at  $V_{\text{rot}} = 95$  km/s, which is within the observed range (Staveley-Smith et al. 2003a; Olsen & Massey 2007; van der Marel et al. 2002).

### 2.3 Orbit of the SMC about the LMC and Definition of Models

Following the method outlined in B10, the MCs are evolved as an isolated interacting binary pair over a period of  $\sim 7$  Gyr since the SMC first crossed within  $R_{200} = 117$  kpc of the LMC.

The SMC is placed on an eccentric orbit about the LMC ( $\text{ecc} = 0.7$ ). Higher orbital eccentricities for the SMC result in fly-by encounters between the MCs, while lower values cause the SMC's orbit to decay too quickly.

The simulation is stopped at characteristic points in time, defining two models for the orbital history of the SMC about the LMC, referred to as Model 1 and Model 2. Model 1 is stopped after 5.1 Gyr and Model 2 after 5.9 Gyr. Thus, Model 1 and 2 differ based on the number of passages the SMC has completed about the LMC. In Model 1, the SMC has completed 2 passages about the LMC, whereas in Model 2 it has completed 3. The stopping times are chosen such that 1 Gyr after this time, the LMC will have travelled from a distance of 220 kpc ( $R_{200}$  for the MW) to its current location and the SMC will have completed the desired number of orbits about the LMC.

The choice of these two models is motivated by the

overarching goal of this study to assess the role of interactions between the MCs to their evolution. Given the chosen L/SMC mass ratio of 1:10, it is unlikely that the SMC could have survived more than 3 passages about the LMC, making Model 2 a maximal interaction scenario. Model 1 is very similar to the solution presented in B10 - the analysis of such a model is a direct extension of the B10 work. Tidal forces between the MCs have been acknowledged as playing an important role in the formation of the Magellanic Stream in many previous studies. In fact, in Connors et al. (2006), the tidal force from the LMC on the SMC dominates over MW tides for most of the SMC's orbit. But to explain the Leading Arm Feature and extent of the Magellanic Stream, MW tides have been invoked in all of these studies. Instead, here and in B10 we illustrate how such extended structures can form without requiring the MCs to complete an orbit about the MW.

The orbit of the SMC about the LMC in Model 1 and Model 2 is plotted in the top panel of Figure 2. The black line indicates the evolution of the system in isolation (no MW potential) and is continued 1 Gyr past the respective stopping point for each model. The red line shows how the orbit of the SMC is modified if instead the binary pair is captured by the MW after the stopping point.

In Model 1, MW tides work to keep the LMC and SMC further apart than they would have been in isolation. In Model 2 the opposite occurs; the MW's gravitational pull forces the SMC to collide directly with the LMC. The distinct outcomes occur because of differences in the SMC's separation from the MW relative to its separation from the LMC at the pericenter of its orbit about the MW. At pericenter, the SMC is closer to the LMC in Model 2 than in Model 1 (see Figure 4).

The bottom panels of Figure 2 show the gas distribution of the L/SMC at the stopping points for each model as contours plotted over the stellar distribution. After 5.1 Gyr (stopping point for Model 1) the SMC is at the apocenter of its second orbit about the LMC. After 5.9 Gyr (stopping point for Model 2) the SMC is just completing its second orbit. As outlined in B10, a tidal bridge and extended tail forms as a result of the action of LMC tides on the SMC; these features form before the system is captured by the MW.

### 2.4 Orbit of the MCs about the MW

At the stopping time (5.1 Gyr for Model 1 and 5.9 Gyr for Model 2), the isolated MC pair is placed at  $R_{200} = 220$  kpc from MW's galactic center, as illustrated in Figure 3 (left panels).  $R_{200}$  is chosen as the starting radius because the MW tidal field does not distort the orbit of the SMC relative to the isolated orbit until well within that radius; it takes 500 Myr for the red and black lines in the top panels of Figure 2 to deviate after the stopping point (i.e. 500 Myr after they cross  $R_{200}$ ). As such, the overall interaction history of the MCs is well-described by the isolated system before this point.

The galaxies travel to their current locations on orbits consistent with the HST proper motions for the LMC, as indicated in Figure 3 (right panels). This takes 1 Gyr in both models since the LMC's orbit about the MW is roughly the same in both cases - it is the SMC's orbit that differs.

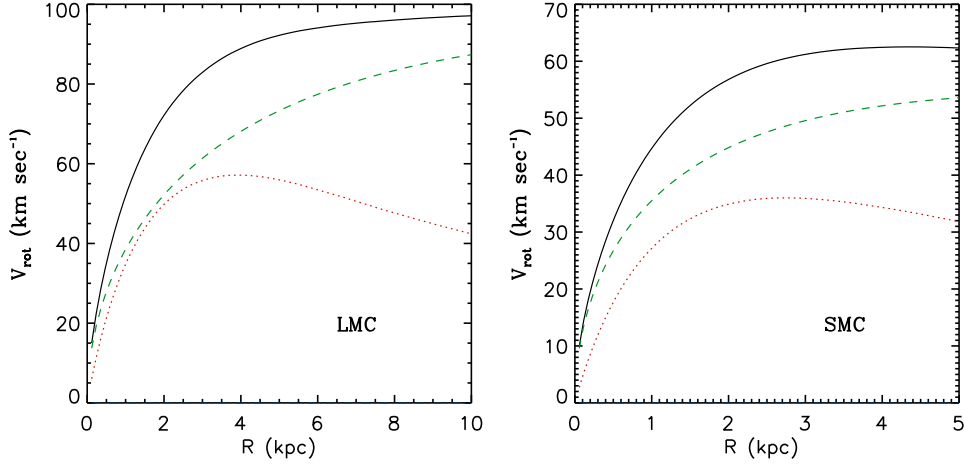


**Figure 1.** The initial rotation curve is plotted for the LMC (left) and SMC (right). The different lines indicate the contribution from the dark matter halo (green, dashed) and the disk (red, dotted). The solid black line indicates the total rotation curve.

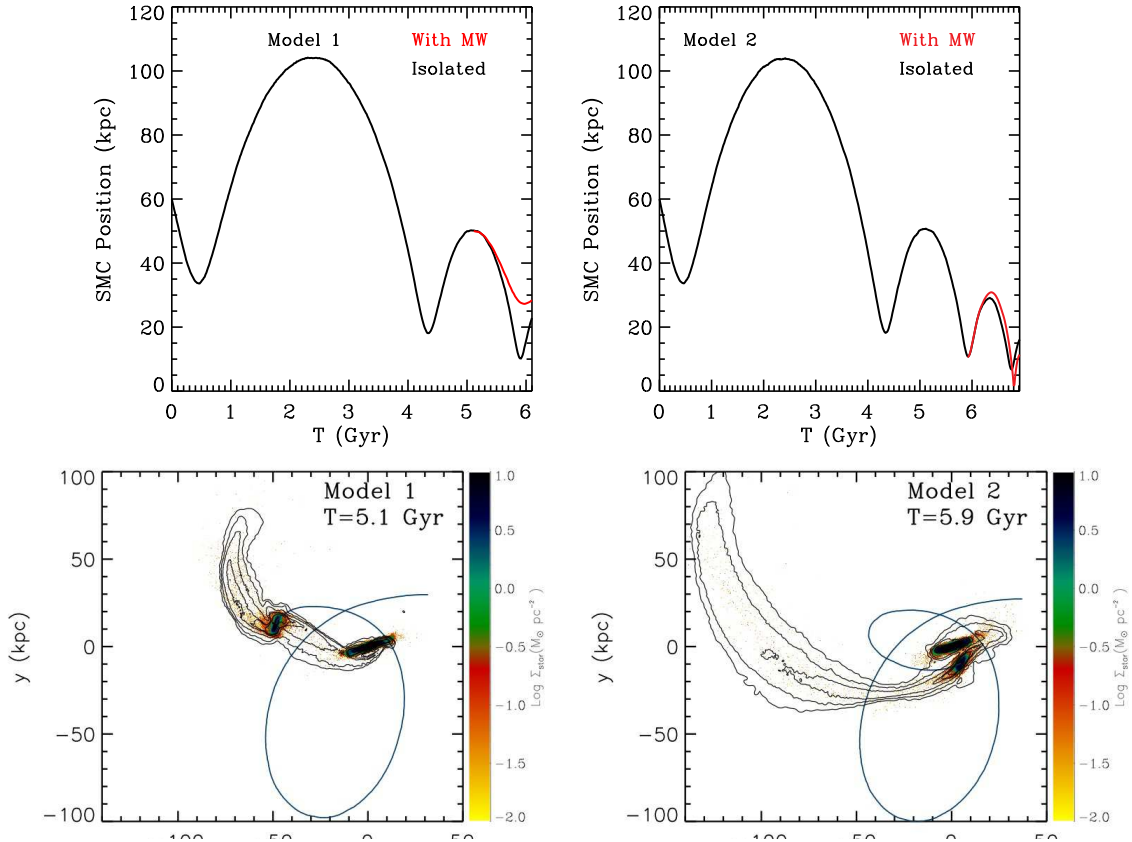


**Figure 2.** *Top Panel:* The separation of the SMC from the LMC is plotted as a function of time for Model 1 (left) and Model 2 (right). The black line denotes the orbital history when the LMC and SMC are modeled as an isolated binary pair: the MW's potential is not included. The red line indicates how the separation between the MCs is modified after the pair first cross within  $R_{200} = 220$  kpc of the MW. This occurs after 5.1 Gyr for Model 1 and after 5.9 Gyr for Model 2; these times are referred to as the stopping times for each model. *Bottom Panel:* The gas column density of the isolated LMC-SMC system is projected in the binary orbital plane as contours over the stellar distribution at the stopping time for Model 1 (left) and Model 2 (right). Gas contours span a range of  $10^{18} - 10^{20} \text{ cm}^{-2}$ , where each contour represents an increase in column density by a factor of 1.5. These images thus depict the gas distribution of the simulated system *before* it is influenced by the MW's gravitational potential. An extended tail of gas is stripped from the SMC and a bridge of gas connects it to the LMC in both models (see also Figure 1 of B10).

**Table 1.** L/SMC Initial Conditions

Property	LMC	SMC
$M_*$ ( $M_\odot$ )	$2.5 \times 10^9$	$2.6 \times 10^{8a}$
$M_{gas}$ ( $M_\odot$ )	$1.1 \times 10^9$	$7.9 \times 10^8$
$f_{gas}^b$	0.3	0.75
$M_{total}$ ( $M_\odot$ ) <sup>c</sup>	$1.8 \times 10^{11}$	$2.1 \times 10^{10}$
$R_{200}$ (kpc) <sup>d</sup>	117.1	57.1
$C$	9	15
$r_S$ (kpc) <sup>e</sup>	13.0	3.8
$r_H$ (kpc) <sup>e</sup>	21.4	7.3
Stellar Disk scale length (kpc)	1.7	1.1 <sup>a</sup>
Gas Disk scale length (kpc)	1.7	3.3
Gravitational Softening Gas/Stars (kpc)	0.1	0.1
Gravitational Softening Halo (kpc)	0.29	0.29
Nstars	$10^6$	$10^5$
Ngas	$3 \times 10^5$	$3 \times 10^5$
Nhalo	$10^5$	$10^4$
$q^f$	0.3	0.3

<sup>a</sup>Note that the initial stellar mass and stellar disk scale length chosen for the SMC deviate from the values adopted in B10. Here the disk is chosen to be more extended in order to increase the number of stars removed by LMC tides. Other changes in parameter values are minor and reflect attempts to match various observed mass constraints for the MCs (see Table 2).

<sup>b</sup>The gas fraction relative to the total disk mass (stars + gas). The gas fractions of isolated dwarf galaxies are known to be large, e.g. Geha et al. (2006)

<sup>c</sup>The total mass of the LMC/SMC at infall is determined using the observed stellar mass of the LMC(SMC)  $M_* = 3 \times 10^9 M_\odot$  ( $3 \times 10^8 M_\odot$ ) (van der Marel et al. 2002; Stanimirović et al. 2004) and the relations from Guo et al. (2010). The total halo mass used to define the Hernquist dark matter profile is then  $M_{halo} = M_{total} - M_* - M_{gas}$ .

<sup>d</sup>The radius where the average enclosed density is 200 times the critical density of the universe

<sup>e</sup>The scale radius for the NFW profile ( $r_S$ ), which is used to define the scale radius of the Hernquist profile ( $r_H$ ), following Springel et al. (2005).

<sup>f</sup>The effective equation of state parameter,  $q$ , defines the pressurization of the ISM following (Springel et al. 2005).

The Galactocentric position and velocities of the MCs are plotted in Figure 4 as a function of time since they first crossed within  $R_{200}$  of the MW. Also plotted are the relative positions and velocities between the MCs (orange line).

In Model 2 the SMC completes an additional passage about the LMC since entering the virial radius, versus in Model 1. This additional passage results in a direct collision between the MCs and the formation of a new bridge. Tidal bridges and tails are formed at each pericentric passage of the SMC about the LMC (Toomre & Toomre 1972). Thus, in Model 2, the bridge connecting the MCs will have formed  $\sim 100$  Myr ago, during this direct collision (separation approaching zero).

## 2.5 Comparison of Modeled Orbits with Data

For each model, the initial velocities and positions of the LMC and SMC at  $R_{200} = 220$  kpc from the MW and their final values today are summarized and compared to data from Kallivayalil et al. (2006a) (hereafter K1) and Kallivayalil et al. (2006b) (hereafter K2) in Table 2. The proper motion error space for the K1 HST proper motion measurements of the LMC is indicated in Figure 5. Over-plotted are various other measurements for the LMC's proper motion and the simulated Model 1 and 2 results. The final LMC velocities and positions are designed to be within  $1\sigma$  of the observations in both models. The differences be-

tween the two models are the orbital parameters for the SMC.

In Model 1 the SMC velocity is significantly larger than that indicated by the HST proper motions of K2. In Model 2, the SMC velocities are in better agreement, however the separation between the LMC and SMC is smaller than observed (by about 10 kpc). As such, the line-of-sight velocity and proper motions for the SMC are also different than observed.

While the SMC velocities and positions are not perfect matches to the observations, it is unlikely that significantly new insight would be gained as to the physical processes at work if an exact solution were found. Slightly different choices of orbital parameters and timing in the orbit can change the SMC's final position and velocity, but not the physical picture. This is practically illustrated by comparing the resulting large-scale gas distribution in Model 1 and 2 (see § 3); despite differences in the SMC orbital properties, the same overall scenario has produced similar global features (i.e. a Leading Arm, Bridge and Stream). To match the exact properties of the Magellanic System, a more detailed study, varying orbital parameters, L/SMC mass ratios, MW mass, etc, is required; this is beyond the scope of the present study.

We have obtained another epoch of data with WFC3, resulting in an average time baseline of 7 years (Kallivayalil et al. in prep). These new data are expected to reduce the

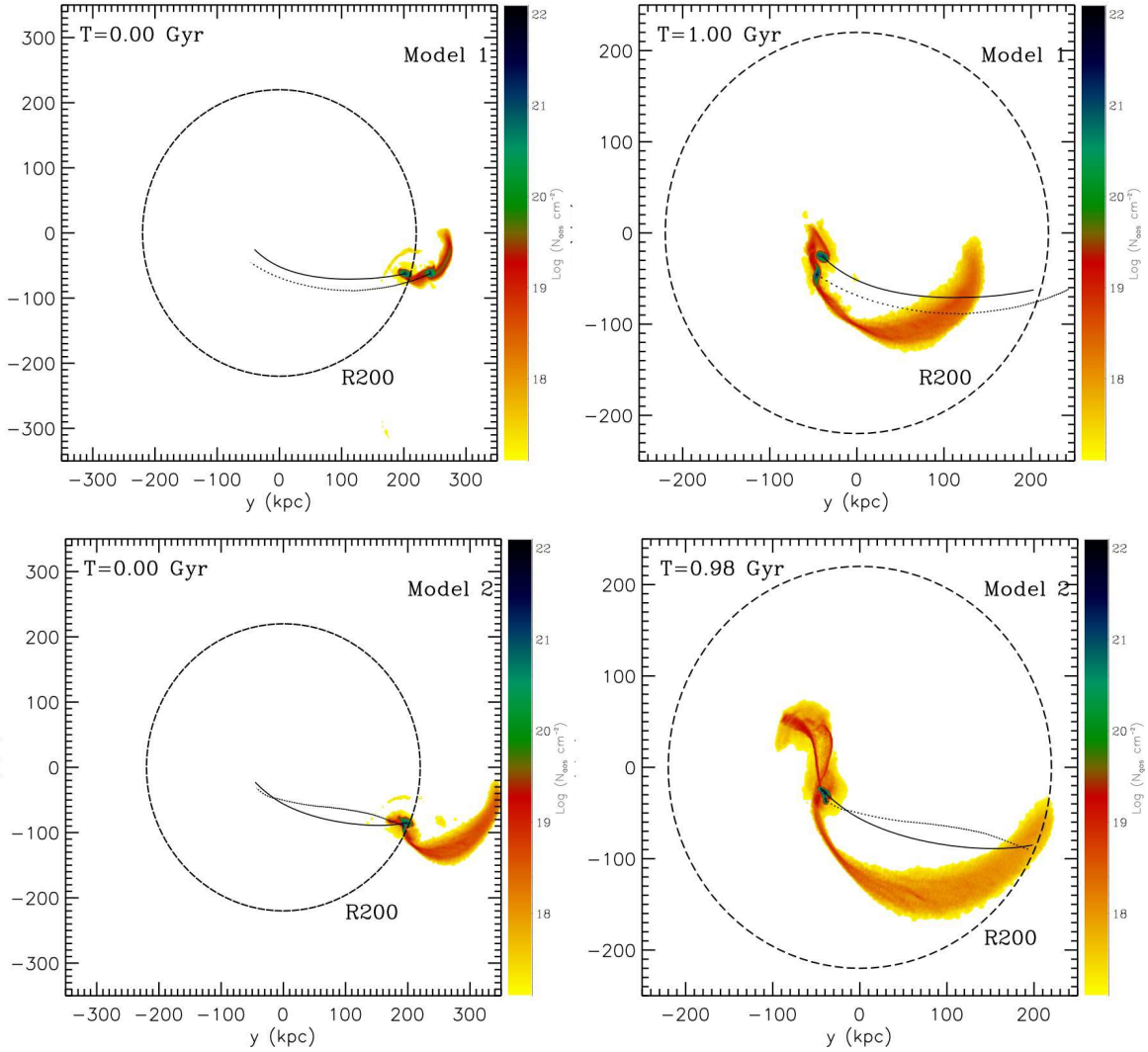


**Figure 3.** Projected gas column densities in the YZ galactocentric plane for the simulated Magellanic System when the LMC first crosses within  $R_{200}$  of the MW (time=0, left) and today (time $\sim$ 1.0 Gyr, right). The circle indicates the location of  $R_{200} = 220$  kpc. The results for Model 1 are plotted in the top row and Model 2 is on the bottom. The LMC's(SMC's) orbital path is denoted by the solid(dashed) line.

errors on the proper motions by a factor of 3, potentially narrowing parameter space the SMC's error space. We note that, within this error space, the exact choice of LMC and SMC velocity today will not alter the physical picture presented in this work, which is that tidal interactions between the two Clouds are the main driver for their morphological and kinematic evolution.

### 3 LARGE SCALE GAS MORPHOLOGY

The resulting large scale gas distributions in Models 1 and 2 are shown in a Hammer-Aitoff projection in Figure 6. In both models, the final gas distribution can be described as an extended tail, a leading component and a bridge of gas connecting the two galaxies. As such, the main components of the Magellanic System are reproduced by both models. Moreover, in both cases the simulated stream stretches  $\sim 150$  degrees across the sky, as observed (Nidever et al. 2008).

In Figure 7 the simulated stream is plotted in Magellanic Coordinates, a variation of the galactic coordinate system where the Stream is straight (Nidever et al. 2008). In both models, the simulated stream deviates away from the projected location of the past orbits on the plane of the sky, as expected according to the recent proper motions (see e.g., Figure 8 in Besla et al. 2007). The deviation is a natural result of the proposed stream formation mechanism. It occurs largely because the Stream is removed in the binary LMC-SMC orbital plane by LMC tides. This binary plane is not parallel to the LMC-SMC-MW orbital plane, thus the Stream is not coincident with the orbit of the MCs about the MW. A second factor is the orientation of the SMC's disk; the location of the simulated stream can be modified by changing this angle. In both of these models the SMC disk is initially oriented 90 degrees with respect to the SMC-LMC orbital plane. The deviation between the simulated stream and the orbits is more pronounced in Model 1 than in Model 2. However, this could be altered if the SMC disk

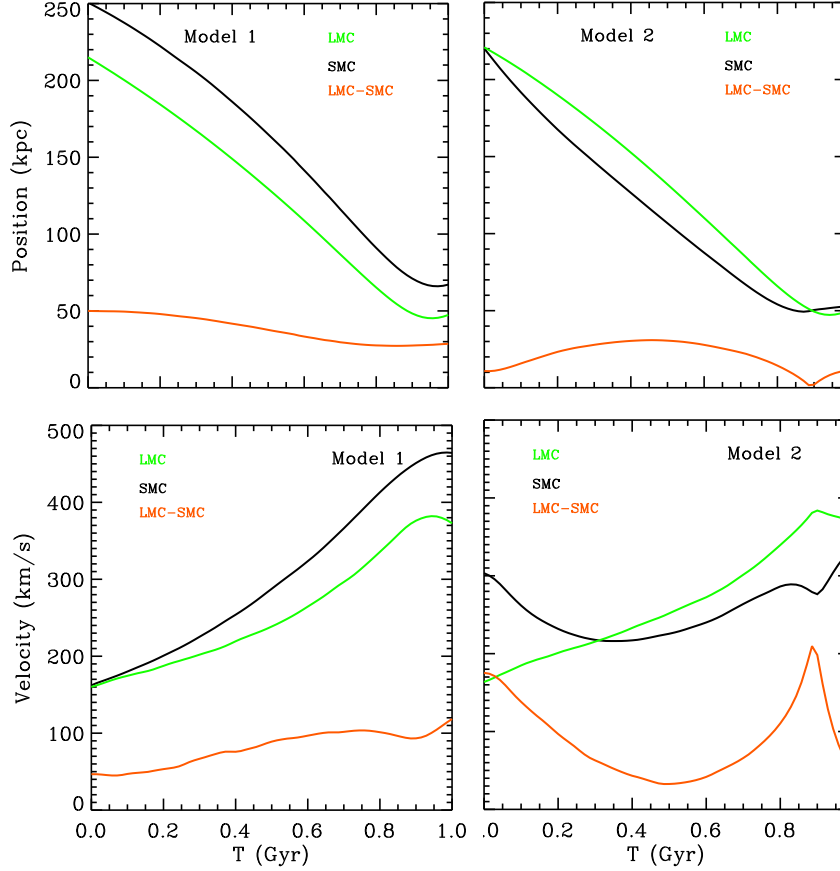


**Figure 4.** The Galactocentric position (top) and velocities (bottom) of the LMC (green) and SMC (black) are plotted as a function of time since the MCs first crossed within  $R_{200} = 220$  kpc of the MW. The relative separation and velocity between the MCs is plotted in orange. The results of Model 1 are plotted in the left column and those of Model 2 are in the right column. The Galactocentric velocities determined by (Kallivayalil et al. 2006a,b, hereafter K1 and K2) are  $378 \pm 18$  km/s for the LMC and  $302 \pm 52$  km/s for the SMC (errors quoted are  $1 \sigma$ ). In Model 1, the velocity of the SMC is higher than observed. In Model 2, the galactocentric position of the SMC is too small (53 kpc vs. 60 kpc); consequently the relative separation between the MCs is also too small (11 kpc vs. 23 kpc). Note that in Model 2, the separation between the LMC and SMC approaches zero  $\sim 100$  Myr ago, indicative of a direct collision.

**Table 2.** Initial and Final Orbital Parameters: Model 1 and 2

Galaxy	Parameter	Model 1		Model 2		Observed Today
		At $R_{200}$	Today	At $R_{200}$	Today	K1 and K2
LMC	(x,y,z) (kpc)	(35, 203, -63)	(-1, -40, -25)	(48, 198, -85)	(-1, -42, -26)	(-0.8, -41.5, -26.9)
	(vx,vy,vz) (kpc)	(-14, -157, -29)	(-72, -267, 250)	(-17, -160, -29)	(-82, -263, 249)	$(-87 \pm 12, -268 \pm 11, 252 \pm 16)$
	$V_{\text{los}}$ (km/s)		262		259	$262 \pm 3.4$
	PM (W, N) (mas/yr)		(-2.02, 0.44)		(-2.03, 0.43)	$(-2.03 \pm 0.08, 0.44 \pm 0.05)$
SMC <sup>a</sup>	position (x,y,z) (kpc)	(5, 243, -62)	(18, -46, -46)	(56, 193, -90)	(6, -39, -35)	(15.3, -36.9, -43.3)
	velocity (vx,vy,vz) (kpc)	(6, -146, -70)	(-88, -384, 246)	(-51, -289, 88)	(-66, -258, 198)	$(-87 \pm 48, -247 \pm 42, 149 \pm 37)$
	$V_{\text{los}}$ (km/s)		215		201	$146 \pm 0.6$

<sup>a</sup> The SMC proper motions are not included in this table: since the line of sight velocities are not well-matched to the observations the proper motions can't be meaningfully compared to the data.

were oriented differently initially and is not a physical distinction between the models; the magnitude of the offset is a tunable parameter. Note that this offset is not expected in a ram pressure solution for the Stream, as the material should be removed along the direction of motion (see Appendix A).

The structure of the Leading Arm Feature (LAF) is distinct in each model. In Model 1 the LAF represents material that was stripped from the SMC on earlier passages and captured by the LMC. Since this material is bound to the LMC it does not extend further than 50 degrees (see Figure 7).



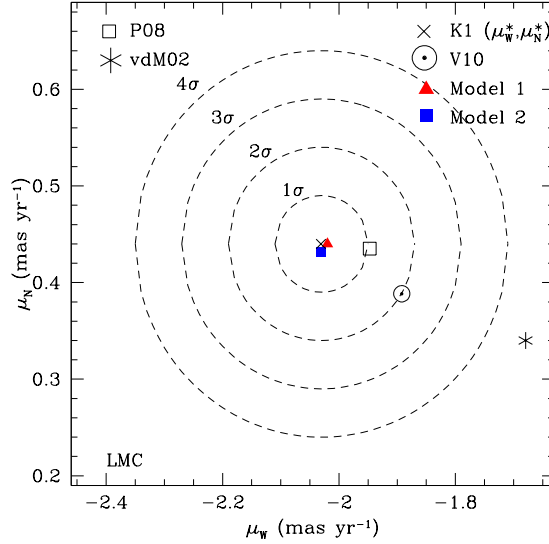


**Figure 5.** Concentric circles indicate the  $4\sigma$  error space for the K1 proper motion error space for the LMC (where the mean value is indicated by the X). The asterisk indicates the mean of all proper motion estimates for the LMC prior to 2002 (van der Marel et al. 2002). The circled dot indicates the recent proper motion estimate by Vieira et al. (2010) and the open square shows the reanalysis of the K1 proper motion data by Piatek et al. (2008). The red triangle and blue square indicate the proper motion of the LMC today in Model 1 and 2, respectively. These values were chosen to closely match the K1 data.

In Model 2, the LAF is better described as a tidal tail or loop, resulting from tidal stripping of the SMC on its most recent orbit about the LMC. The tidal tail gains energy and deviates to larger distances away from the SMC's orbit (e.g., Choi et al. 2007). The resulting simulated LAF in Model 2 spans 80-90 degrees across the sky, which is larger than observed. Unlike the Stream, this material is leading to the MCs and so will experience a significant ram pressure headwind. Consequently, its final appearance, position and angular extent on the plane of the sky cannot be well captured without including hydrodynamic effects (see Appendix A, Binney & Fraternali 2011). Model 2 does illustrate, however, that the observed 70 degree span of the LAF (Nidever et al. 2010) can be reproduced without invoking a previous orbit about the MW.

The Magellanic Stream is observed to have a pronounced HI column density gradient along its extent (Nidever et al. 2010; Putman et al. 2003; Brüns et al. 2005). The maximum gas column density along the simulated Magellanic System is determined from Figure 7 and plotted as a function of Magellanic Longitude in Figure 8. Both models underestimate the observed values, which are indicated by the solid red line (Brüns et al. 2005). There are a number of possible explanations for this discrepancy. This problem could be alleviated if the gas reservoir in the SMC were depleted less efficiently at earlier times; for example, if the SMC's gas disk were initially less extended or if star formation was not quite so efficient. Ram pressure stripping has also not been modeled and could also increase the amount of gas removed as the MCs get closer to the MW. Furthermore, hydrodynamic instabilities are not well modeled with SPH (Agertz et al. 2007; Sijacki et al. 2011), and so clumping of the gas is not captured in these simulations. This is a process

that will clearly influence the resulting gas column density in the Stream (Bland-Hawthorn et al. 2007; Nigra et al. 2010).

At the same time, there are notable consistencies between the models and the data. Nidever et al. (2010) find that the column density along the LAF is fairly constant along its  $\sim 70$  degree span ( $\sim 4 \times 10^{19} \text{ cm}^{-2}$ ); this is true of Model 2. The column density in the bridge in Model 2 also matches the observations: the maximum column density in the Bridge is  $1.64 \times 10^{21} \text{ cm}^{-2}$  (Brüns et al. 2005); the simulated bridge column density for Model 1 is too low. Also in Model 2 the simulated column density of the SMC is higher than that of the LMC, as observed (Brüns et al. 2005, the maximum column density is  $5.45 \times 10^{21} \text{ cm}^{-2}$  and  $9.98 \times 10^{21} \text{ cm}^{-2}$  for the LMC and SMC, respectively).

There is a well-defined velocity gradient along the length of the Stream (Putman et al. 2003; Nidever et al. 2008), ranging from 200 km/s near the Clouds to -400 km/s. The simulated results are plotted in Figure 9 for both models. The observed line-of-sight velocities along the MS (yellow line) and the rest of the system are well-traced by Model 1. Model 2 also reproduces the observed range of velocities, but the slope of the velocity gradient along the MS is not well-matched to the data.

Given that the only difference between Model 1 and Model 2 is the SMC's orbital parameters, it is doubtful that this discrepancy in predicted velocities owes to missing physics. Rather, a detailed search of the SMC's orbital parameter space will likely yield better matches for Model 2. It is possible that gas drag effects (not modeled here) may also modify the velocity profile - particularly in the LAF, where the velocities are currently too high in Model 2.

No direct distance measures exist for the Magellanic Stream, as no stellar counterpart has yet been identified (Guhathakurta & Reitzel 1998). Jin & Lynden-Bell (2008)

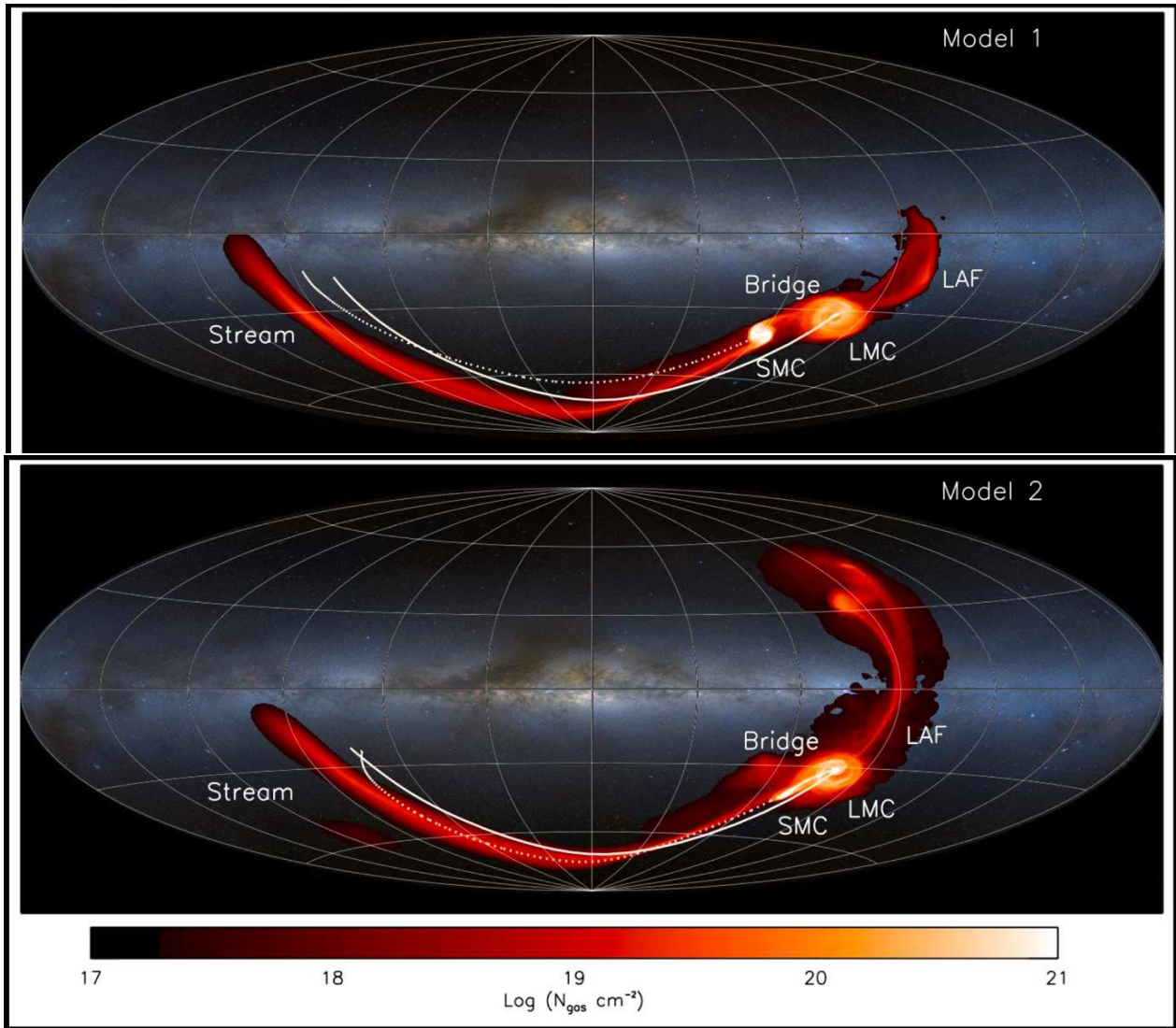


**Figure 6.** Hammer-Aitoff projection of the total gas distribution of the simulated Magellanic System (red scale) for Model 1 (top) and Model 2 (bottom) is plotted over an image of the MW (blue, white and brown colors; Mellinger 2009). The orbital trajectory of the LMC(SMC) is indicated by the solid(dotted) white line. Various components of the Magellanic System are labelled, where LAF stands for Leading Arm Feature.

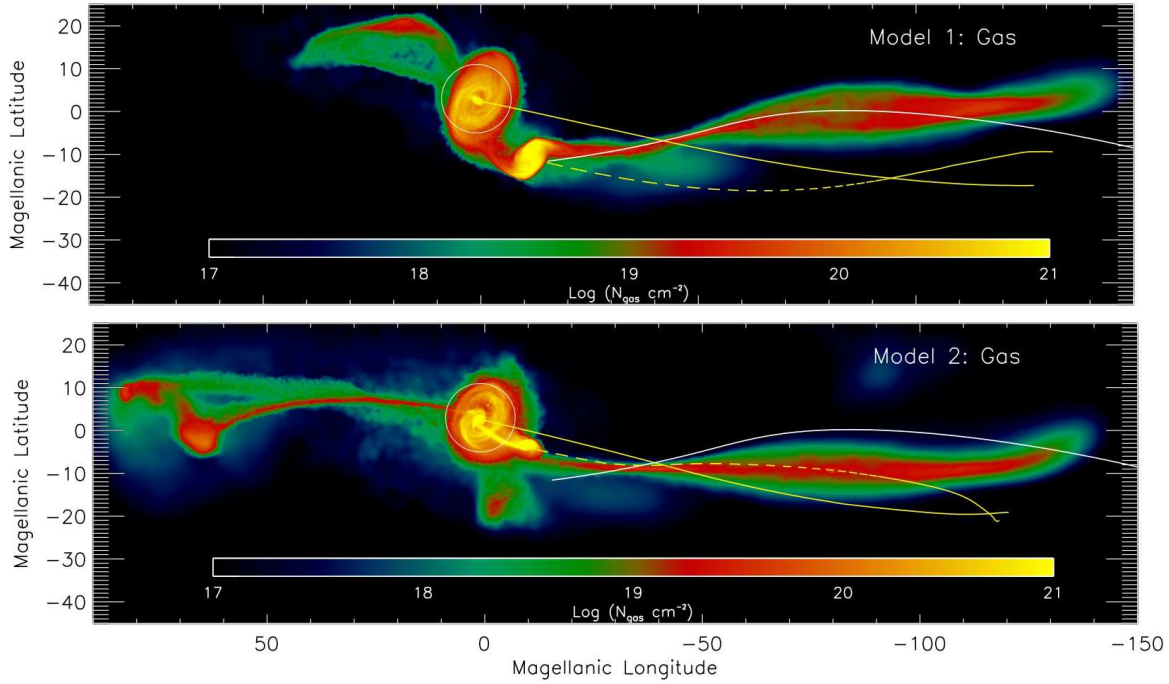
present a geometrical method to determine distances along streams with well defined velocity gradients. Using this method they find the tip of the 100 degree long Stream defined in Putman et al. (2003) (i.e. not including the extension recently described by Nidever et al. 2010) to be located at 75 kpc from the Galactic center. The line-of-sight distances of the gas in the simulated Magellanic System are plotted in Figure 10. The stream produced by Model 1 is generally closer (80-150 kpc) than that of Model 2 (80-230 kpc). Both simulated streams are further away than predicted by the Jin & Lynden-Bell (2008) method; however, gas drag and changes in the model parameters (such as increasing the MW mass) can alter the distance to the simulated stream.

#### 4 LMC MORPHOLOGY

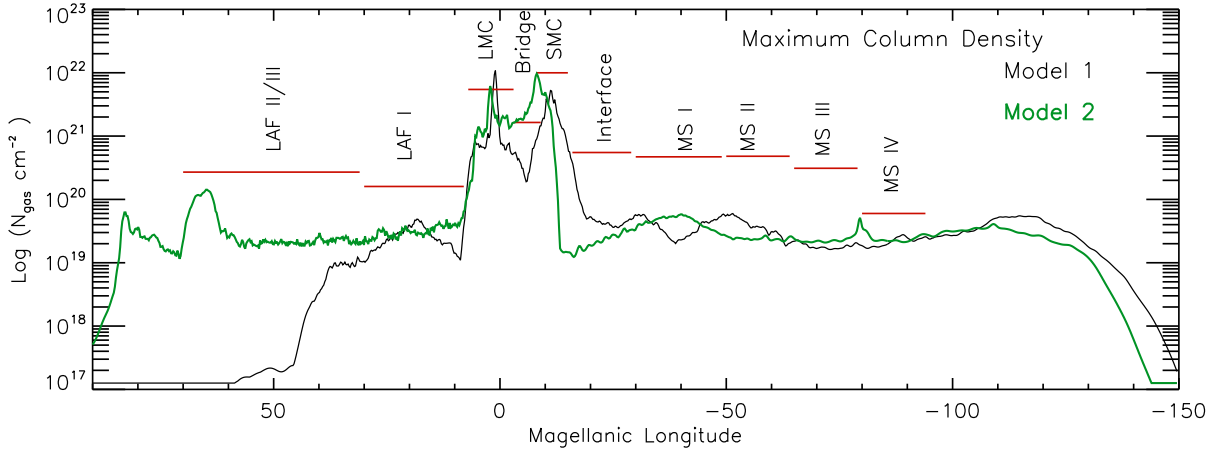
In this section we study in detail the resulting structure of the simulated LMC stellar and gaseous disks in our two models of the large scale gas distribution of the Magellanic System.

Figure 11 shows the LMC's stellar disk in Model 1 (left) and Model 2 (right) in our line-of-sight view. The RA and DEC coordinate grid is overplotted in green across the face of the disk. In both models the LMC disk is inclined  $\sim 35$  degrees with respect to the plane of the sky, as observed (i.e. despite the recent collision of the SMC in Model 2, the inclination of the LMC's disk remains unchanged).

The Model 1 disk is fairly uniform and symmetric. In Model 2, however, there are perturbations induced in the LMC's stellar disk by the recent encounter with the SMC. In particular, there are significant distortions in the North-East. Only LMC stellar particles are plotted in these images,



**Figure 7.** The total gas distribution of the simulated Magellanic System for Model 1 (top) and Model 2 (bottom) is plotted in Magellanic Coordinates. The orbital trajectory of the LMC(SMC) is indicated by the solid(dashed) yellow line. The actual location of the Magellanic Stream is roughly traced by the solid white line. The white circle represents the observed radius of the LMC.



**Figure 8.** The maximum total gas column density of the simulated Magellanic System is plotted as a function of Magellanic Longitude for Model 1 (black line) and Model 2 (green thick line). The red lines indicate the observed maximum HI column density from the Brüns et al. (2005) data set for each marked region: MS stands for Magellanic Stream and LAF for Leading Arm Feature. The various roman numerals refer to specific sections of the MS/LAF as defined in Putman et al. (2003) and Brüns et al. (2005). Neither model reproduces the observed HI column density gradient in the MS.

and so these structures are in the plane of the LMC disk and do not represent tidal debris from the SMC. Such structures are observed in deep observations of the periphery of the LMC's disk (de Vaucouleurs & Freeman 1972, Martinez-Delgado et al. in prep).

The initial LMC disk was bar unstable, and so the bar feature in both models was present since the beginning of the simulation - it was not induced by external tidal perturbations from the SMC or MW. Interestingly, in Model 2,

the bar of the LMC is now off-centered relative to the disk, as observed. No such perturbations are observed in Model 1: without a close encounter the LMC looks like a symmetric spiral disk galaxy and it is doubtful that such a galaxy would be classified as a Magellanic Irregular galaxy.

In Figures 12 and 13 we take a closer look at the LMC's gas and stellar disk by deprojecting the disk from the line-of-sight frame into a Cartesian coordinate system centered on the LMC disk plane for both Model 1 and Model 2. Only

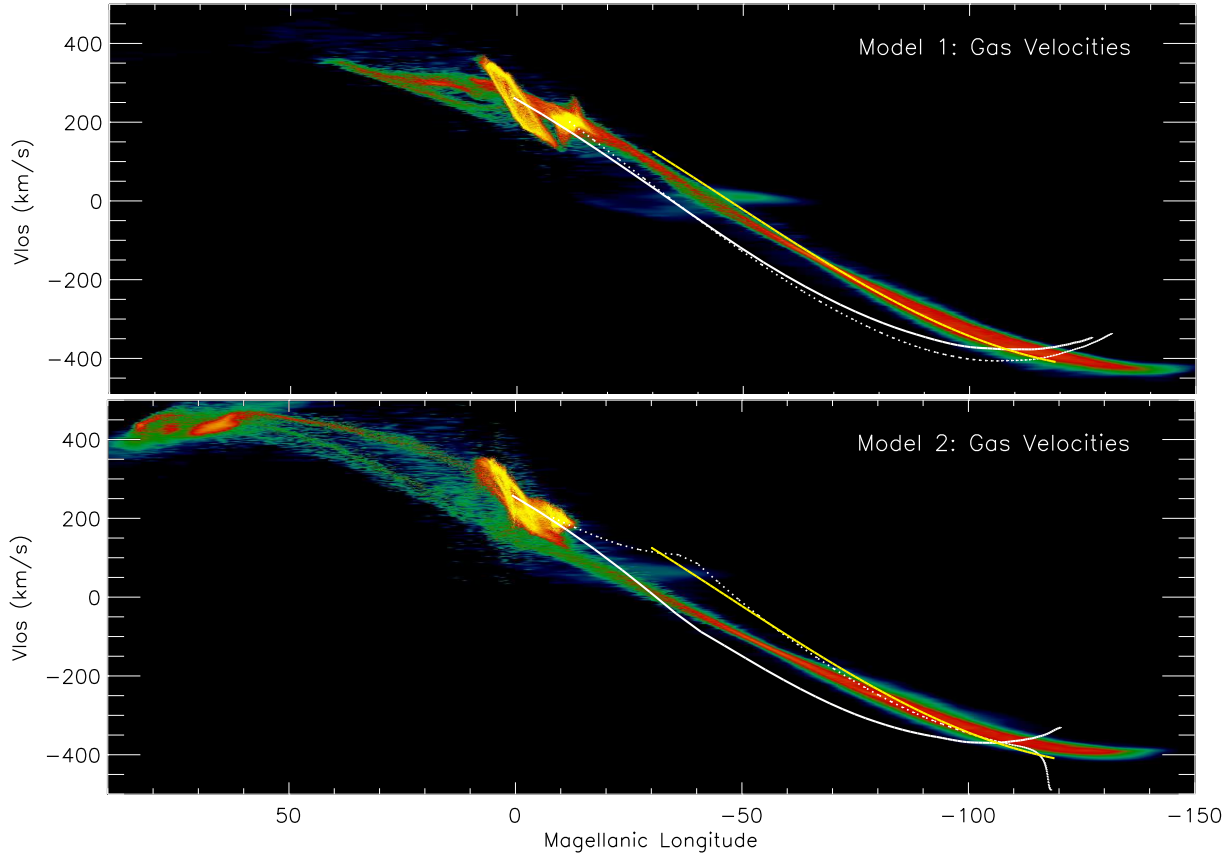


**Figure 9.** The line-of-sight velocities for the total gas distribution of the simulated Magellanic System are plotted as a function of Magellanic Longitude for Model 1 (top) and Model 2 (bottom). The yellow line is a fit to the data of Nidever et al. (2010). The modeled line-of-sight velocities along the past orbit of the LMC(SMC) are plotted as the solid (dotted) white line.

particles associated with the LMC are plotted. The images are centered on the peak of the stellar density distribution (i.e. the photometric center).

In Model 1, the bar of the LMC is clearly visible in both the stellar and gaseous disks. This is in disagreement with the observed HI maps of Kim et al. (1998): there is no distinguishable bar structure in the observed global HI emission that is comparable to the optical bar. The results for Model 2 illustrate the consequences of a recent (100-300 Myr ago) direct collision between the LMC and SMC. In this scenario, Model 1 represents the state of the LMC disk before the collision occurred, where the LMC is a symmetric barred spiral. After the collision, the bar has become off-centered with respect to the underlying disk and it has almost disappeared from the gas disk of the LMC. The reason becomes clear when the disk is viewed edge-on along the x-axis. The bar has become warped by  $\sim 10$ -15 degrees relative to the LMC disk plane and is therefore inefficient at funneling gas in the way it could in Model 1. This warp of the bar is less extreme than that required by models such as Zhao & Evans (2000) for the microlensing optical depth and may be consistent with the observations of Subramaniam & Subramaniam (2009). The simulated offset bar is also consistent with the structure of the observed bar, which is described as a cigar shaped structure with dimensions of  $1 \times 3$  kpc.

From the edge-on view of the Model 2 gas disk, it is clear that LMC gas particles have been pulled out of the

disk by the passage of the SMC through the LMC. This causes the appearance of a gaseous “arm” in the face-on view of the disk. Such “arms” are seen in the LMC gaseous disk (Kim et al. 1998) and are believed to be related to the Magellanic Bridge and Leading Arm Feature (Nidever et al. 2008). In our interpretation, at least one of these “arms” is extra-planar and located behind the LMC disk. The fact that LMC gas is removed from the disk towards the Bridge indicates that the formation of the Magellanic Bridge has been aided by hydrodynamic gas drag. It is not purely a tidal feature. The Bridge is known to be quite metal poor along two sightlines towards early type stars (see Table B1 and Lehner et al. 2008). However, a full census of the metallicity across the Bridge does not yet exist. Regardless, it is clear that LMC gas cannot have contaminated the entirety of the Bridge. The Model 2 scenario predicts that the majority of the Bridge material originated from the SMC, but there should be some contribution from LMC gas that increases in importance with proximity to the LMC. Model 2 thus predicts that Bridge material towards the LMC should be increasingly metal enriched. This should not be true in Model 1.

In the edge-on view of the Model 1 disk, the gas disk appears to be tilted relative to the stellar distribution. This is likely because of the infall of gas from the SMC that forms the Magellanic Bridge. The outer stellar and gas disks in Model 2 are significantly warped and distorted in the edge-



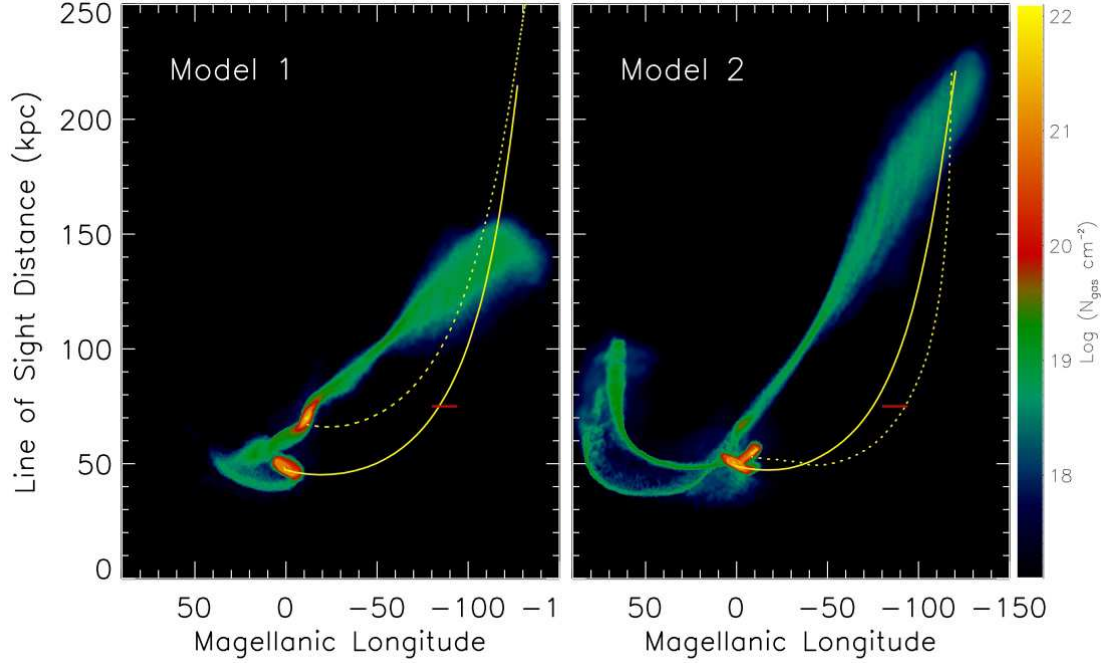


**Figure 10.** The line-of-sight distances for the gas distribution of the simulated system are plotted as a function of Magellanic Longitude for Model 1 (left) and Model 2 (right). The modeled line-of-sight distance along the orbit of the LMC(SMC) is plotted as the solid (dashed) yellow line. The solid red line indicates the distance estimate from Jin & Lynden-Bell (2008).

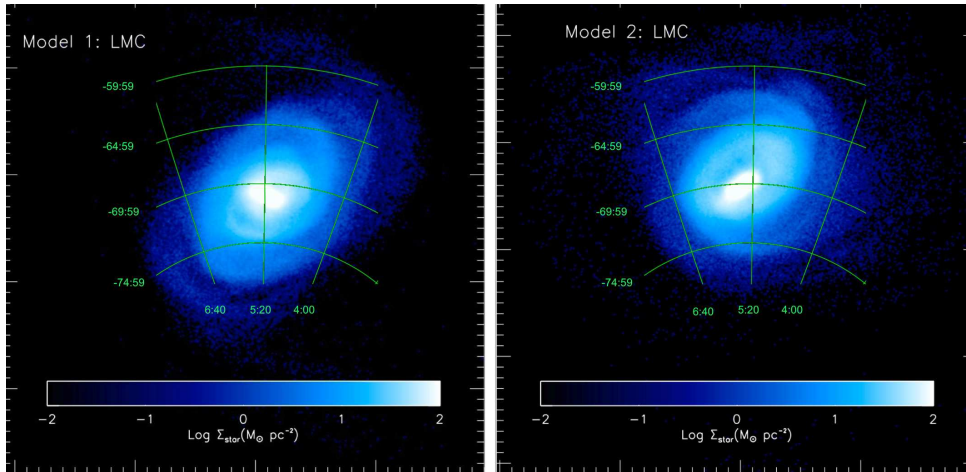


**Figure 11.** The stellar surface density of the LMC disk is plotted in the line-of-sight frame for Model 1 (top) and Model 2 (bottom). RA and DEC grids are overlaid in green across the face of the disk. The stellar distribution in Model 2 is significantly more disturbed than in Model 1. In particular, the bar in Model 2 is off-center relative to the stellar disk. The Model 2 LMC disk is also significantly disturbed in the upper left (North-East).

on view. The true disk is also observed to be both flared (Alves & Nelson 2000) and warped (van der Marel & Cioni 2001; Olsen & Salyk 2002; Nikolaev et al. 2004). Such results are in keeping with a study of Magellanic-type spirals by Wilcots et al. (1996), who also suggest that the observed lopsidedness in their HI disks may be a result of minor mergers.

In Model 2 the gas disk has also formed a pronounced

arc in the upper right. Since our star formation prescriptions depend sensitively on the gas density, this arc of gas will also be actively forming stars (see § 6.1), giving the LMC the appearance of a one-armed spiral. A number of numerical studies have been conducted on the resulting structure of a large galaxy after a direct collision with a smaller companion in the context of explaining the origin of ring galaxies (Lynds & Toomre 1976; Weil & Hernquist 1993; Struck

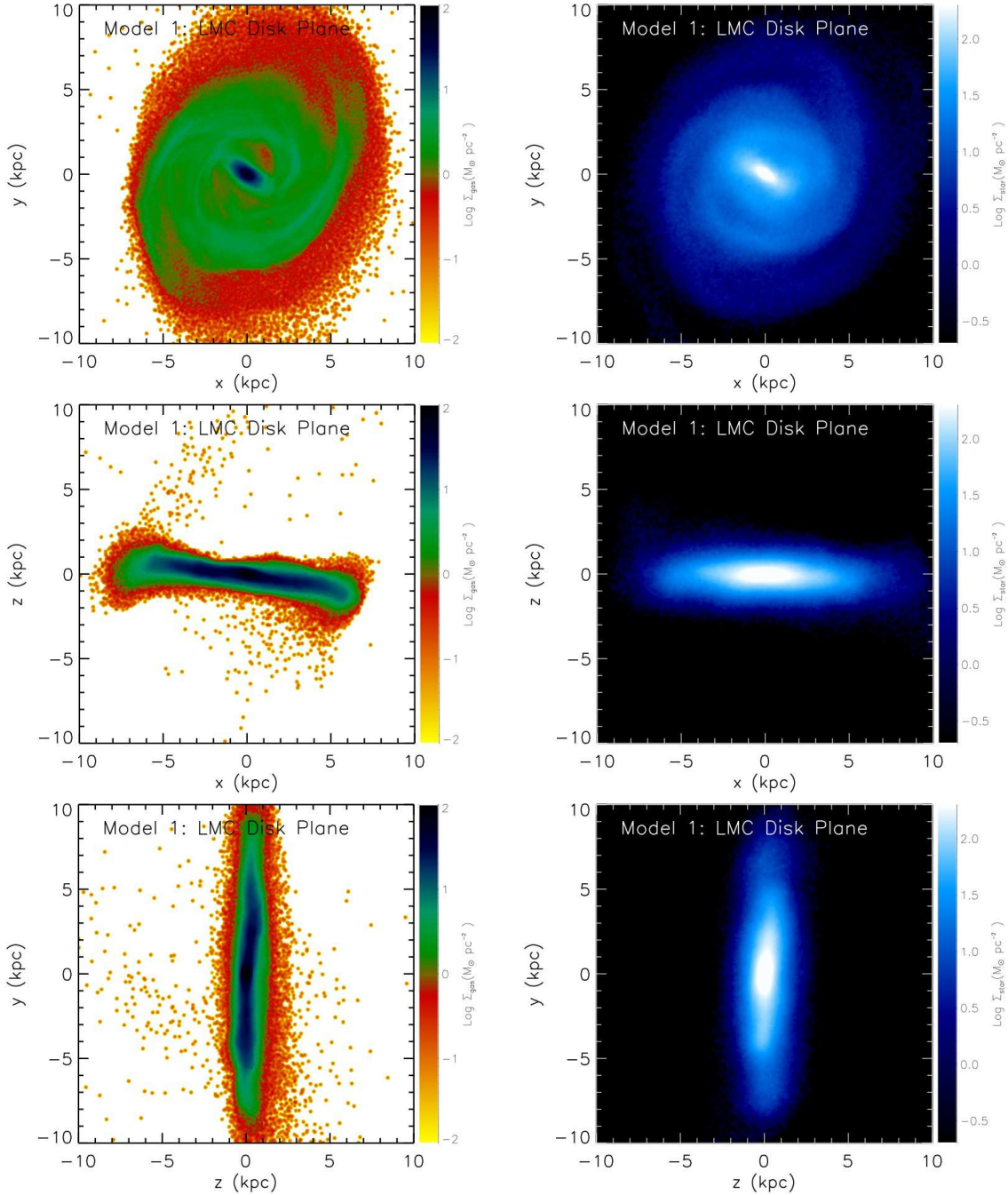


**Figure 12.** The gas (left) and stellar (right) density of the LMC disk for Model 1. *Top*: face-on view ( $x, y$  plane). *Middle*: edge-on view along the  $x$  axis. *Bottom*: along the  $y$  axis. Both the gas and stellar projections have a centered, in-plane bar.

1997). In particular, Struck (1997) finds that, in some cases, a one-armed spiral structure can be excited in the larger galaxy. Also, Bekki (2009) explored a scenario where the LMC bar becomes off-center as a result of a recent encounter with a dark  $10^8 M_\odot$  companion. The specific asymmetries induced depend sensitively on the mass ratio, inclination and the location of the smaller companion’s passage through the larger galaxy. A future study will explore these parameters in depth in the context of the LMC-SMC encounter and assess the longevity of the resulting asymmetric structures. For example, Levine & Sparke (1998) have illustrated that

disk-lopsidedness can be long-lived if the disk is displaced from the center of the dark matter potential and spinning in a sense that is retrograde to its orbit about that center.

Finally we note that, while we have not discussed the results for the SMC in detail, the simulated SMC morphology in Model 2 is consistent with the observations of a “bar”-like main body with a stellar wing leading towards the LMC and a significant line-of-sight depth. We will discuss these results in depth in a future paper (Besla et al. 2012 in prep.).

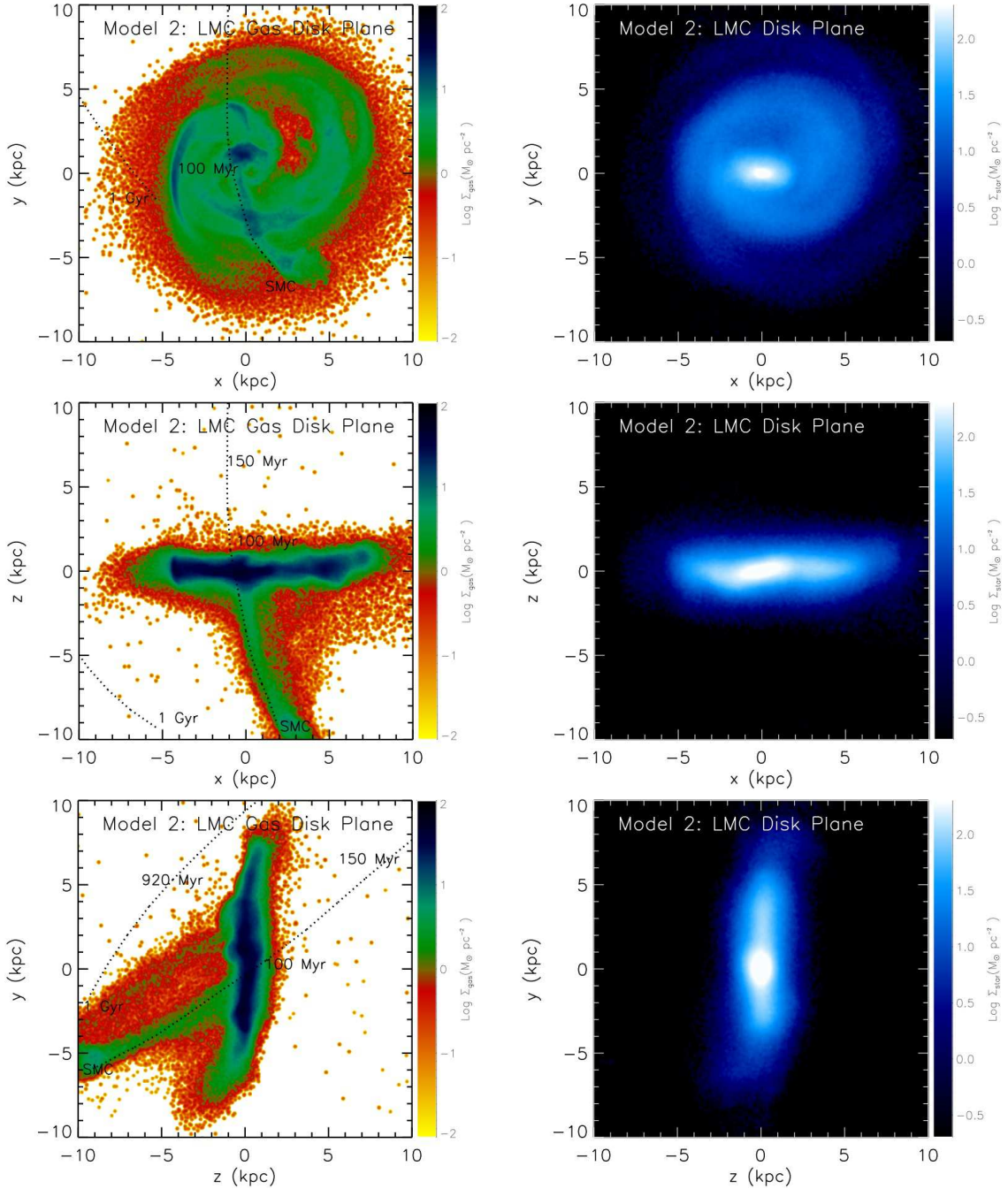


**Figure 13.** Same as Figure 12 but for Model 2. The stellar bar is clearly off-centered and warped relative to the stellar disk; it is also absent in the gas. The SMC’s orbit in an LMC-centric frame is overplotted (dashed line) in the middle and bottom panels of the LMC’s gas distribution. Various times are also marked along the SMC’s past orbit. The SMC collides with the LMC 100 Myr ago and the SMC’s current position is marked. An extra-planar stream of gas is pulled out from the LMC by the passage of the SMC.

## 5 LMC KINEMATICS

The internal kinematics of the LMC has been quantified by many tracers. The LMC’s rotation curve rises roughly linearly to a radius of  $\sim 4$  kpc, after which it stays flat at a value of  $V_{rot}$ . The observed rotation curve has been noted to peak at different values depending on the kinematic tracer being studied. The HI kinematics yield  $V_{rot} = 80$  km/s (Staveley-Smith et al. 2003a), data from red su-

pergiants gives  $V_{rot} = 107$  km/s (Olsen & Massey 2007) and carbon stars yields  $V_{rot}=61$  km/s (van der Marel et al. 2002). However, recently Olsen et al. (2011) examined the kinematics of a combined population of massive red supergiants, oxygen-rich and carbon-rich AGB stars in the LMC. After correcting for the LMC’s space motion and the asymmetric drift in the AGB population, they find a consistent rotation curve between all kinematic tracers with  $V_{rot} = 87$

$\pm 5$  km/s. This is in accord with the HI rotation curve and the initial value adopted in this study ( $\sim 95$  km/s).

The LMC disk initial conditions (gas fraction, equation of state) are chosen such that the LMC kinematics are representative of a symmetric, bar-unstable disk galaxy. It remains to be seen whether MW tides will introduce kinematic anomalies in the disk in a first infall scenario, or, perhaps more significantly, whether the LMC can retain a kinematically stable disk after a direct collision with the SMC (i.e. in Model 2).

In Figures 14 and 15 the kinematics of the LMC disk in Models 1 and 2, respectively, are broken down for various kinematic tracers: gas (top panel), young stars (middle) and old stars (bottom), in the line-of-sight frame. In each panel the disk is centered on the stellar center of mass. The center panels show the surface density of the tracer population. A slit is placed along the largest velocity gradient of the LMC's older stellar distribution and is defined as the major kinematic axis (red). A second slit is placed 90 degrees with respect to the major axis and referred to as the "minor" kinematic axis (blue). The position angle of the kinematic major axis of the simulated disk for Model 1 is 55 degrees counter-clockwise from the x-axis in all panels and 50 degrees for Model 2. The line-of-sight velocities along the slits are plotted in the left panel. The right panel shows the full line-of-sight velocity field. The middle and right boxes are 18 kpc a side whereas the left box is scaled to the length of the slit (16 kpc along the x-axis).

In both models the LMC disk retains a pronounced velocity gradient along the same major axis; perhaps surprisingly, the LMC disk retains a well defined rotation curve despite a direct collision with the SMC. Indeed, Hopkins et al. (2008, 2009) showed that disks can survive even a 1:1 mass ratio major merger. However, the disk kinematics in Model 2 are more distorted than in Model 1, particularly the 0 velocity field.

There are observed asymmetries in the LMC's gas and stellar kinematics. It has long been noted that the HI kinematic center is offset by  $\sim 1$  kpc from *both* the stellar kinematic and photometric center, which is roughly centered on the stellar bar (as illustrated in Cole et al. 2005). However, upcoming work by Kallivayalil et al. (in prep) using a 3rd epoch of HST data provides proper motions of high enough accuracy to independently constrain all parameters of the LMC rotation field and geometry, including the dynamical center. The best-fit stellar dynamical center from the proper motions *agrees* with the HI dynamical center determined by Kim et al. (1998), but remains offset from the photometric center (van der Marel & Kallivayalil, in prep.).

Each panel in Figures 14 and 15 is centered on the peak of the stellar density of the simulated LMC disk; i.e. the photometric center. In Model 1, the stellar density peak is coincident with the kinematic centers of all tracers (vertical dashed line in left panel crosses zero where the major slit velocities do). Thus, contrary to observations, the stellar and gas kinematic centers are coincident with the photometric center and the center of the stellar bar.

In Model 2, the zero velocity field of the stars and gas is twisted such that the velocity gradient does not cross zero at the location of the stellar density peak. The kinematic centers of all tracers are offset by about 1 kpc from the photometric centers, as observed. However, the gas and stellar

kinematics are somewhat discrepant from each other. This is illustrated by placing a third slit 1 kpc above the major axis (illustrated in the right hand panel of Figure 15, in green). The old and young stellar line-of-sight velocities along this slit are similar to those along the original major axis. The gas line-of-sight velocities, on the other hand, have changed, crossing the zero axis roughly 1 kpc further away than seen for the stars. This implies that the shape of the zero velocity field across the face of the gaseous and stellar disks are different and is likely a result of the warped stellar bar. Note that neither model predicts strong differences in the rotation curves traced by the young ( $< 1$  Gyr) and older stellar populations, as expected from Olsen et al. (2011).

Again, the simulated SMC kinematics will be presented in a forthcoming paper. However, we mention here that the resulting kinematics are much more consistent with Model 2 than Model 1. It appears that a direct collision with the LMC is required to erase the initial velocity gradient in the older stellar population. Zaritsky et al. (2000) was unable to find a pronounced velocity gradient in the RGB population within a radius of 2 kpc of the center of mass, despite the existence of a 60 km/s velocity gradient in the gas (Stanimirović et al. 2004). In our simulations, the gas is able to cool, since it is dissipative, and the original gas disk survives the tidal shocks resulting from the direct impact with the LMC, whereas the older stellar population does not. In Model 1 (no direct impact with the LMC), there is always a pronounced gradient in both the stellar and gaseous components of the SMC.

## 6 DISCUSSION

In this study we have shown that it is possible to explain the nature of the LMC's off-center stellar bar (§ 4) and gas and stellar kinematics (§ 5) in a model that self-consistently reproduces the general large scale gas morphology of the Magellanic System (§ 3) in a first infall scenario. To do this, we invoked a recent direct collision between the LMC and SMC (Model 2). Here we discuss some of the testable consequences of such a scenario.

Note that the resulting simulated SMC kinematics and structure and an expected stellar counterpart to the Magellanic Stream will be discussed in upcoming papers.

### 6.1 The Recent Star Formation History of MCs

A direct recent collision between the LMC and SMC would likely leave notable marks in the star formation histories (SFHs) of both of these galaxies. A correlated burst of star formation during such a recent encounter has been theorized in many previous numerical studies (e.g., Gardiner & Noguchi 1996; Bekki & Chiba 2005, 2007). Observationally, there is significant debate over the existence of correlated bursts of star formation within both galaxies. Harris & Zaritsky (2009) claim that the total SFR in the LMC was higher than average  $\sim 100$  and 500 Myr ago and in the SMC at  $\sim 60$  and 400 Myr ago. Other authors claim that the LMC shows global enhancements  $\sim 125$  and 800 Myr ago (Pietrzynski & Udalski 2000a) and in the SMC at  $\sim 100$  Myr only (Pietrzynski & Udalski 2000b). The general consensus does appear to be that both galaxies show a steadily



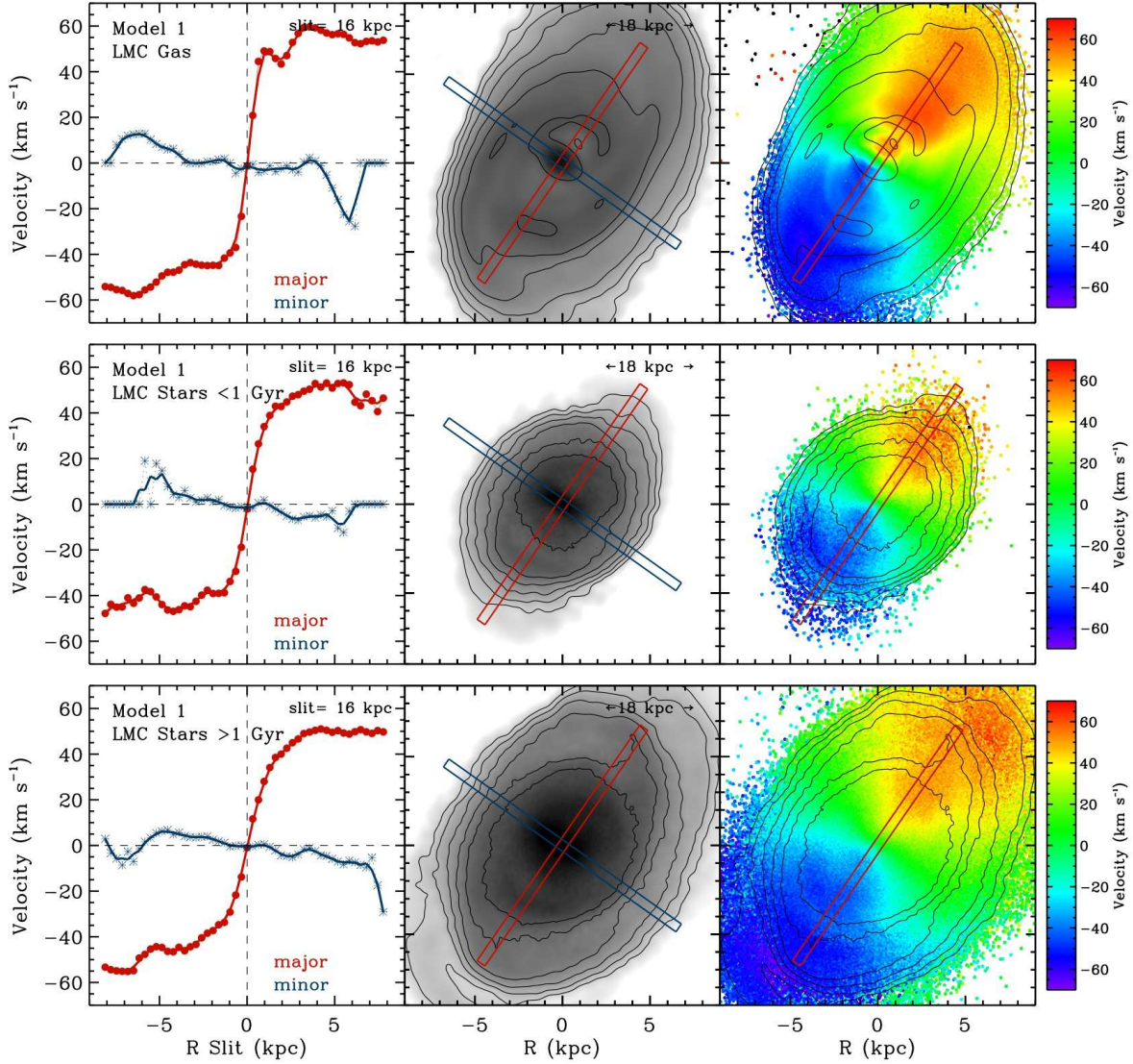


**Figure 14.** The kinematics of the simulated LMC’s gaseous disk (top), young stellar disk ( $< 1$  Gyr; middle) and old stellar disk ( $> 1$  Gyr; bottom) in Model 1 are illustrated in the line-of-sight frame (North to the top, East to the left; the SMC is located to the South-West). The *right panels* show the line-of-sight velocity field, where the center-of-mass velocity of the respective kinematic tracer has been subtracted. Density contours and major axis slit location are also indicated. The color gradient denotes material moving towards (blue) and away (red) from the observer. The *central panels* show the surface density of the tracer, with density contours overplotted. The central and right panel boxes spans 18 kpc a side. Each box is centered on the stellar density peak. Slits are placed along the major (red) and minor (blue) stellar kinematic axes as indicated. The major kinematic axis slit is inclined 55 degrees counter clock wise from the x-axis in all panels. The minor kinematic axis is placed 90 degrees with respect to the major axis, although in practice this does not exactly trace the zero velocity regions. Note that even if the gas kinematics are being examined, the red slits still denote the locations of the *stellar* kinematic axes. In the *left panel*, the line-of-sight velocities are plotted along the slit. The dashed vertical line indicates the location of the peak stellar density (photometric center); in Model 1 it is coincident with the kinematic centers of all tracers.

increasing SFR over the past Gyr (Harris & Zaritsky 2009; Noël et al. 2009; McCumber et al. 2005). Testing this scenario reliably depends on the accuracy of the timing of the collision/interactions between the L/SMC and the adopted star formation prescriptions.

We can bracket the time range for this impact to be within 100-300 Myr. The upper limit on the collision timescale comes from the oldest detected stellar populations in the Magellanic Bridge, which are believed to form in-situ (Harris 2007) and thus mark the formation time of the

Bridge. As such, given the model parameter uncertainties, we cannot use the models here to definitively predict the timing of the collision and consequent star formation.

The exact timing of the collision is strongly dependent on model parameters. In the presented Model 2, the most recent collision occurred  $\sim 100$  Myr ago. However, the MCs are too close together today in this model, indicating that the true collision likely occurred earlier.

Given our adopted prescriptions, the modeled SFHs of both MCs are plotted as a function of time since they first

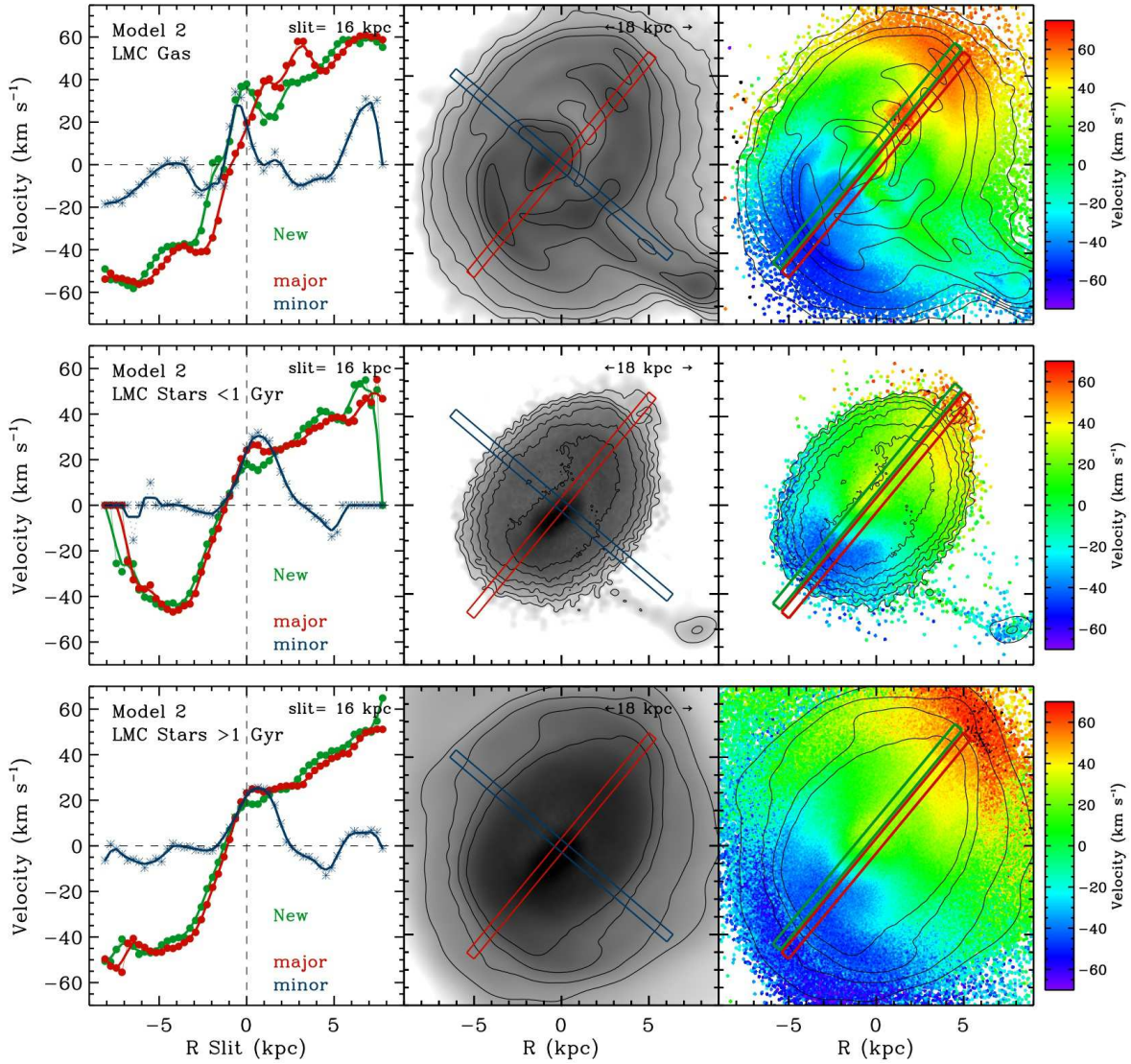


**Figure 15.** The same as in Figure 14, except for Model 2. The kinematic major axis (red) is inclined 50 degrees counter clock wise from the x-axis in all panels. In the left panel it is clear that the kinematic center of all tracer populations are coincident, but not with the photometric center (dashed vertical line). Furthermore, the shape of the velocity field as traced by gas vs. stars is different across the face of the disk. This is illustrated by the inclusion of a new slit (in green), placed 1 kpc above the major axis. The line-of-sight velocities of the gas along the 'New' slit deviate from their stellar counterpart. This offset is likely a result of the warped stellar bar.

**Table 3.** Current Star Formation Rate

Galaxy	Model 1 ( $M_{\odot}/\text{yr}$ )	Model 2 ( $M_{\odot}/\text{yr}$ )	H $\alpha$ & IR ( $M_{\odot}/\text{yr}$ )	Free-free Emission ( $M_{\odot}/\text{yr}$ )
LMC	0.5	0.4	0.25	0.14
SMC	0.2	0.4	0.05-0.08	0.015

Note. — The SFR is computed within a radius of 15 kpc for the LMC and 2 kpc for the SMC. The third column indicates the mean values determined from H $\alpha$  and MIPS emission by Whitney et al. (2008) for the LMC and from IR and H $\alpha$  by Wilke et al. (2004) and Kennicutt & Hodge (1986), respectively. The fourth column presents a lower limit, determined from the free-free flux measured by Murray & Rahman (2010) using WMAP.

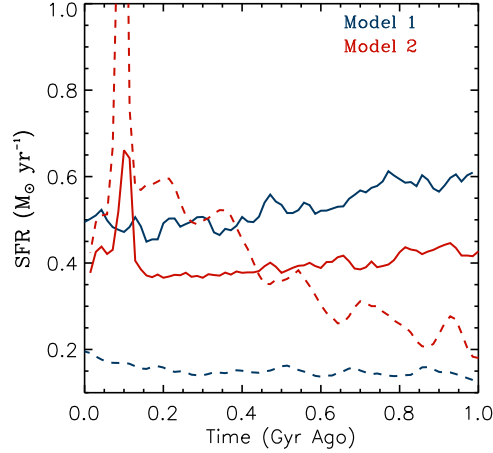


**Figure 16.** The simulated SFR is computed within a radius of 15 kpc for the LMC (solid lines) and 2 kpc for the SMC (dashed lines) and plotted as a function of time since the MCs first crossed within  $R_{200}$  of the MW for Model 1 (red) and Model 2 (blue). The corresponding orbital histories are plotted in Figure 4. In Model 2, the MCs experience a close encounter at 0.1 Gyr ago (time 0 indicates today).

crossed within  $R_{200}$  of the MW in Figure 16. Note that the star formation rate is derived from the gas density above a set threshold value. Contrary to Model 1, the SFH of the SMC over the past Gyr in Model 2 increases steadily, as observed (Noël et al. 2009; McCumber et al. 2005). The Model 2 result occurs because the separation between the MCs is smaller than in Model 1, hence the relative importance of tidal distortions from the LMC and consequent triggered star formation is also stronger.

The LMC is observed to be unusually blue relative to analogs with similar R-band magnitudes identified in SDSS (Tollerud et al. 2011). This is likely a result of two factors: 1) if the MCs are on their first infall and just past their first pericentric approach to our MW, they may be experiencing triggered star formation induced by MW tides. 2) Interactions between the MCs have likely kept the SFR in the LMC higher than it would be if it did not have a companion. The SFRs of galaxies are known to increase as a function of separation to a close companion (Larson & Tinsley 1978; Freedman Woods et al. 2010; Patton et al. 2011, and references therein). Since LMC-SMC pairs are rarely found around MW type hosts (Liu et al. 2011; Boylan-Kolchin et al. 2011), it is natural that the LMC should have an anomalously high current SFR relative to the average analog (which is more likely to be isolated). This theory can be tested by comparing the LMC’s color/SFR to a sample of Magellanic Irregulars (LMC analogs) with known close companions.

The recent collision between the MCs in Model 2 results in a dramatic increase in the SFR in the SMC at that time. As discussed above, the exact timing of the true collision is quite uncertain. The magnitude of the simulated burst is inconsistent with observations of the SFH of the SMC (Harris & Zaritsky 2006). Furthermore, the modeled SFRs today are also higher in both MCs than observed (see Table 3). This likely points to significant problems in our adopted star formation prescriptions.

The star formation prescription we have adopted in these simulations follows a Kennicutt-Schmidt volume density law with a local volume density cutoff for star for-

mation of  $n_H = 0.13 \text{ cm}^{-3}$ . Springel & Hernquist (2003) showed that when combined with appropriate star formation timescales and typical scale-heights this gives a good match to the observed Kennicutt star formation surface density relation for relatively massive galaxies. However in the regime where galactic gas is dominated by atomic hydrogen and where molecular, star forming, gas constitutes only a fraction of the gaseous content, one has to properly account for the formation of local density enhancements and molecular hydrogen formation (Robertson & Kravtsov 2008; Kuhlen et al. 2011; Krumholz et al. 2009; Hopkins et al. 2011). In low mass galaxies that tend to be metal poor, such as the SMC (Fox et al. 2010), molecular gas formation and therefore also the star formation is very inefficient. Theoretical models show that not accounting for the details of molecular gas formation and using global metallicity independent, low density, threshold for the ISM model can lead to serious overestimates of the star formation rates of metal-poor galaxies (Kuhlen et al. 2011). While larger improvement can be made by accounting for metallicity dependent molecular gas formation in sub-resolution models, direct modeling of processes that self-regulate formation of molecular clouds, their star formation and related feedback requires more a complex ISM model and resolution that is beyond the simulations used in this work (Hopkins et al. 2011).

Since the bulk of this study focuses on the morphological and kinematic properties of the simulated MCs and the dynamics of the Magellanic System, the detailed star formation prescription does not alter any of the main conclusions in this work. However, it does limit the predictive power of the models concerning the chemical evolution and SFHs of the MCs. Future detailed studies of star formation prescriptions/feedback in a repeated series of Model 2 collisions can be compared directly with the multiples observational data sets for the SFHs of the MCs. Such a study may be a powerful method of constraining the appropriate sub-resolution physics for Magellanic Irregulars and shed light on to the nature of bursts of star formation in the histories of the MCs.



## 6.2 Star Formation in the Bridge and Stream

An additional check for our proposed Models is the predicted locations of ongoing star formation in the simulated Magellanic Bridge and Stream.

Figure 17 shows the instantaneous SFR density in the Magellanic System for Models 1 and 2; the SFR density is derived from the gas density. These plots indicate the location of gas with densities above the star formation threshold and should thus be forming stars. While these plots may not be quantitatively accurate (the results clearly depend on the star formation prescription), they do highlight the location of high density gas that should be forming stars in any sub-grid model.

In both cases the gas densities in the Magellanic Stream are too low to form stars. This is consistent with observations; molecular gas has not been detected in the densest cloudlets of the Stream, suggesting that star formation is not actively occurring there (Matthews et al. 2009).

In Model 1 stars do not form in the Magellanic Bridge, whereas in Model 2 a well-defined bridge of star forming gas is seen connecting both galaxies. Stars as young as 10-40 Myr have been detected in the Bridge (Demers & Battinelli 1998), indicating that star formation is on-going there, as these stars could not have migrated from the SMC during their lifetimes. Furthermore, Harris (2007) was unable to locate stars older than 300 Myr in the Bridge, lending support to the idea that the majority of young stars there were formed in-situ. The different results between Model 1 and Model 2 indicate that a very close/direct encounter between the MCs may be required in order to trigger in-situ star formation in the Bridge, otherwise gas densities in the tidal bridge should not be significantly different from the Magellanic Stream (i.e. the tidal tail). A close encounter has generally been invoked to explain the properties of the Bridge in previous studies (e.g., Yoshizawa & Noguchi 2003; Connors et al. 2006). Clearly shock induced star formation is a relevant process in the direct collision scenario presented here and must be accounted for in order to characterize this environment accurately.

Note that, although these results seem to favor Model 2, ram pressure compression of the Bridge region may also lead to triggered star formation (e.g., Mastropietro et al. 2009). Although, in this case there likely should be stars forming in both the Leading Arm and the Magellanic Stream as well.

The SFR along the Bridge in Model 2 increases steadily towards the SMC; this should be testable observationally. Indeed, Harris (2007) showed that the distribution of blue stars is more dense in the Bridge towards the SMC. Spitzer observations also confirm the presence of young stars in the “wing” of the SMC, which leads to the Bridge (Gordon et al. 2009). Furthermore, H $\alpha$  measurements of the Bridge by the Wisconsin H $\alpha$  Mapper (WHAM) survey indicate that the H $\alpha$  emission in the Bridge increases steadily towards the SMC (Barger et al. in prep).

In Figure 17 the bar region of Model 1 is currently the dominant site of ongoing star formation in the LMC (contrary to observations). The distribution of star formation in the disk appears similar to an isolated galaxy with a number of spiral arms. On the other hand, in Model 2 the bar is not the most prominent site of star formation today. Figure 18 provides a zoomed in view of the Model 2 results

in the line-of-sight frame for the LMC disk. The center of mass of the stellar disk is located just to the right of an intense star-forming knot that indicates the impact location of the SMC-LMC collision. As discussed earlier, this occurs because the bar is warped with respect to the gas disk plane and is therefore inefficient at funneling gas along it.

Without appropriate feedback prescriptions the appearance of the impact site today is difficult to assess. The thickness of the gas disk near the impact site has increased relative to the rest of the disk (see where the SMC’s trajectory crosses the LMC disk plane in Figure 13). Intriguingly, this is also true of the active 30 Doradus star forming region (Padoan et al. 2001), which is located at roughly the same location. However, the SFH of the true 30 Doradus region indicates that it has only been an active site of star formation for the past 12 Myr (Harris & Zaritsky 2009). Without accurately capturing star formation induced by shocks and including feedback, it is unclear whether the initial collision (100-300 Myr ago) is related to the triggering of star formation in 30 Doradus today or whether its remnant is related to any of the supergiant shells in the LMC disk (Kim et al. 1998; Book et al. 2008, 2009).

## 6.3 Mass Breakdown

The initial and final mass contained within characteristic radii of the simulated LMC and SMC and the resulting mass of the simulated stream are listed in Table 4 and compared with observations. Quoted gas mass estimates are for the *total* gas component; the neutral HI content will be lower than these values. We do not include a UV ionization model in these simulations and thus cannot accurately estimate the neutral gas fraction.

In general, the mass estimates for the LMC and SMC agree with the observations within a factor of two. However, the final gas mass estimates for the MCs are lower than those observed and the simulated stream is about a factor of five lower.

As discussed in § 6.1, given the adopted star formation prescriptions, the SFR in the MCs is being overestimated in the simulations. As a result, the gas consumption timescale is also overestimated. The adoption of different prescriptions and/or changes in model parameters so that the SMC does not lose as much gas at early times (e.g. by reducing the scale length of the SMC’s gas disk) may allow for the SMC to retain its gas for longer, allowing more material to be removed at later times.

The mass budget of the Stream is also likely underestimated because ram pressure stripping has not been modeled here; the bulk of the missing material is in the region closest to the MCs, rather than the tip of the tail. But this still means that more gas needs to be retained by the MCs themselves to provide a gas reservoir for this process to operate at late times. This suggests that the larger problem here is the adopted star formation prescriptions.

Probably more significantly, the total initial gas budget of the MCs has been underestimated in these simulations; the amount of gas initially modeled in both the LMC and SMC cannot explain the total gas budget (including both neutral and *ionized* components) of the Magellanic System. Although the neutral HI gas content of the observed Magellanic System has been well quantified, the ionized gas frac-

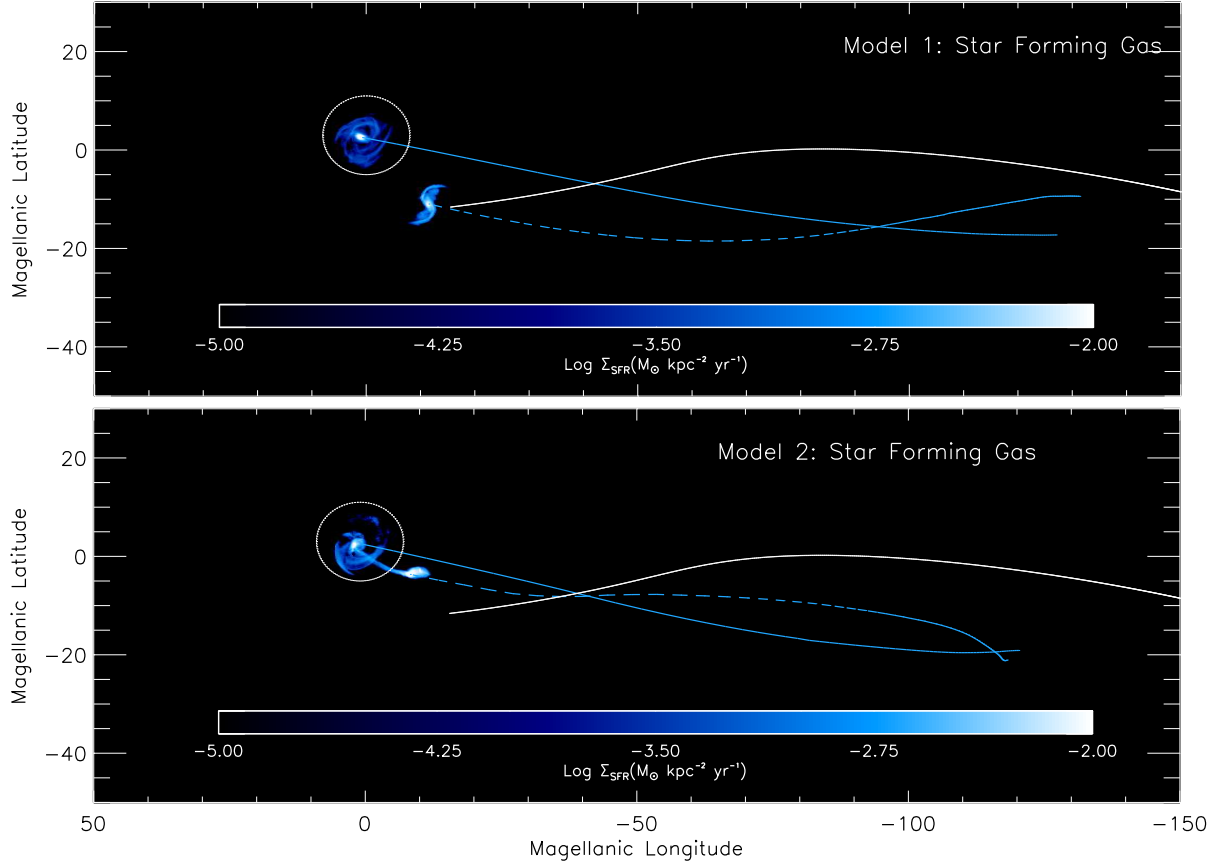


**Figure 17.** The instantaneous SFR density for the simulated Magellanic System is plotted for Model 1 (top panel) and Model 2 (bottom) as a function of Magellanic Longitude. The SFR density is proportional to UV luminosity and identifies the location of gas that is currently forming stars. The white circle indicates the observed extent of the LMC's disk and the solid white line denotes the observed location of the Stream. Blue solid(dashed) lines indicate the past orbits of center of mass of the LMC(SMC).

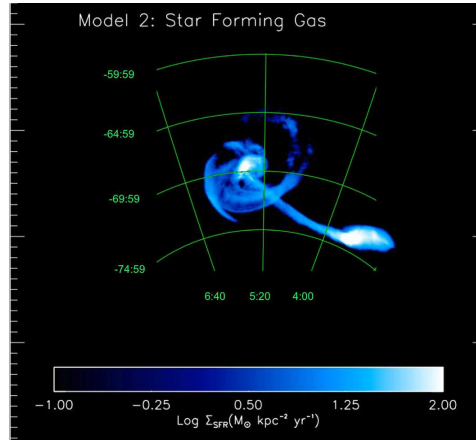


**Figure 18.** A zoom-in on the instantaneous SFR density in the LMC and SMC in Model 2 from the bottom panel of Figure 17. RA and DEC grids are overplotted in green (North is to the top and East is to the left). This image indicates where stars are expected to be forming in the LMC *today*: star forming gas is concentrated in the South-East and a single spiral arm of star formation is seen in the North-West. The SFR increases along the simulated bridge towards the SMC (South-East).

tion is poorly understood. Fox et al. (2010) find that at the tip of the Stream as much as 95% of the gas may be ionized. Along a similar line, Lehner et al. (2008) find that gas in the Magellanic Bridge is 70-90 % ionized. This means that the total gas mass budget of the Stream (and consequently of its progenitor) is significantly underestimated. Note that this statement implies that the LMC and SMC must have a significant amount of dark matter in order to make their initial baryon fractions consistent with cosmological expectations; this is the main motivation for the large total infall masses adopted in this study.

The fact that the stellar mass in the central regions of the SMC does not change substantially indicates that the bulk of the material being removed from the SMC via LMC tides is from the outskirts of the SMC. This explains why the stellar counterpart of the Stream is so faint. We will comment on the observability of the this stellar stream counterpart in an upcoming paper.

#### 6.4 Tidally Captured SMC Stars

In the presented models there is a continual transfer of material from the SMC to the LMC. In particular, there is expected to be a population of stars that are tidally stripped from the SMC and captured by the LMC in both models.

Recently, Olsen et al. (2011) discovered a population of metal poor RGB stars in the LMC field that have different kinematics from those of local stars in the LMC disk. Graff et al. (2000) have also identified a possible kinematically distinct collection of carbon stars and suggest that this population lies outside of the LMC. The discovery of such stars is a natural theoretical expectation from any tidal model for the LMC-SMC interaction. To date, no stars have been detected in the Magellanic Stream (Guhathakurta & Reitzel 1998) and only stars younger than 300 Myr have been identified in the Bridge (Harris 2007). Note that the Harris (2007) observations focused on the leading ridgeline (location of the highest gas density) of the Magellanic Bridge. This leading edge would currently be experiencing maximal ram pressure and so it is possible that the peak gas density in the bridge is displaced from the tidal stellar population theorized to be there. Harris (2007) constrained the stellar density of a possible offset stellar population using 2MASS observations, but the 2MASS sensitivity limit of 20 Ks mag/arcsec<sup>2</sup> is likely far too low to detect the expected faint stellar bridge (>30 Ks mag/arcsec<sup>2</sup>; Besla et al. in prep).

The potential identification of tidally stripped SMC stars in orbit about the LMC may be a key discriminant between various model interpretations of the origin of the Magellanic Stream, as they should not be present in a pure hydrodynamic model (Mastropietro et al. 2005) or one that relies on stellar outflows (Nidever et al. 2008; Olano 2004).

To test whether the simulation results for the tidal debris are consistent with the Olsen et al. (2011) detections, we plot in Figure 19 the expected distribution and kinematics of the stars captured by the LMC from the SMC for both Model 1 (top panel) and Model 2 (bottom panel). The box size and orientation is the same as in Figures 14 and 15, that is, the field of view is centered on the LMC. The stellar line-of-sight velocities have been corrected for the center of mass motion of the LMC. The SMC is located towards

the South-West in this viewing perspective. Note that the SMC is actually present in this field-of-view for the Model 2 results, as this simulation resulted in the MCs being closer together than observed.

In Model 1 these transferred stars form a well-defined arc that is in orbit about the LMC: these stars are located behind the LMC disk. Comparing the velocity field to the bottom-right panel of Figure 14, the kinematics of these stars appear to be offset by nearly 90 degrees relative to the velocity gradient in the LMC's disk. In Model 2, the stellar debris from the SMC exhibits a large range in velocities ( $\pm 150$  km/s). We made a velocity floor and ceiling of  $\pm 70$  km/s to better compare to the LMC stellar disk kinematics. In the North-West there are stars that appear to be moving towards the observer and in the South-East there are stars moving away from the observer - this is opposite to the observed kinematics of the LMC stellar disk. Thus in both models, stellar debris captured by the LMC from the SMC is expected to have kinematics that are distinct from those of the LMC disk stars - this is a generic prediction of the B10 model and is consistent with the Olsen et al. (2011) observations.

Olsen et al. (2011) estimate the mass of the observed SMC debris population to be 5% of that of the LMC's current disk mass (i.e.  $\sim 1.4 \times 10^8 M_\odot$ ). In Model 1, only a modest amount of stars is transferred from the SMC to the LMC ( $\sim 0.2\%$ ). As such, Model 1 cannot account for this population. On the other hand, in Model 2, the LMC accretes 1.5% of its current disk mass from the SMC.

The exact distribution of SMC debris is certainly dependent on a number of parameters, but overall we can conclude that the Olsen et al. (2011) results support a model in which LMC tides have been actively distorting the SMC. Furthermore, in both models the accreted stars are largely located behind the LMC disk and may provide a natural explanation for the origin of the observed MACHO microlensing events (Besla et al. in prep).

#### 6.5 The Nature of Magellanic Irregulars

Dwarf galaxies are broadly referred to as galaxies with luminosities  $< 0.1-0.3$  of  $L_*$ . This definition encompasses a wide range of objects of varying morphology, including both the LMC and SMC. In this work we have introduced a mass model for the LMC with a total mass of  $\sim 10^{11} M_\odot$ ; it is questionable as to whether such a massive galaxy should be included in the same category as dwarf Spheroidal or dwarf Irregulars galaxies. In particular, detailed analysis of the geometry (van der Marel & Cioni 2001) and kinematics (van der Marel et al. 2002) of the LMC prove that it is a disk galaxy. Furthermore, when looking at the distribution of intermediate-age and old stars out to large radii (i.e. ignoring the visible light in the bar region), the LMC does not look at all irregular, but clearly resembles a spiral galaxy with an asymmetric one-armed spiral (van der Marel 2001).

de Vaucouleurs & Freeman (1972) suggested that Magellanic Irregulars have more in common with spiral galaxies than dwarfs, referring to the LMC as an asymmetric, late-type barred spiral galaxy. They argue that Magellanic Irregulars represent an extension of the Hubble spiral sequence (Sa, Sb, Sc, Sd, Sm, Im), where the subscript m denotes "Magellanic" (see also, section 4.1.1 of Binney & Merrifield

**Table 4.** Initial and Final Mass Distributions

Galaxy	Property	Initial ( $10^9 M_\odot$ )	Model 1 ( $10^9 M_\odot$ )	Model 2 ( $10^9 M_\odot$ )	Observed ( $10^9 M_\odot$ )
LMC	Stars (< 9 kpc)	2.5	3.1	3.1	2.7 (1)
	Gas (< 5 kpc)	0.87	0.17	0.26	0.441 (2)
	Total (<9 kpc)	18	21	21	13( $\pm 3$ ) (3)
	Total (<4 kpc)	6.9	7.3	7.1	5 (4)
SMC	Stars(< 3 kpc)	0.20	0.26	0.20	0.31 (5)
	Gas (< 3 kpc)	0.20	0.16	0.18	0.42 (5)
	Total (< 3 kpc)	2.1	1.8	1.1	2.7 – 5.1 (6)
	Total(< 1.6 kpc)	0.84	0.70	0.49	2.4 (4) 1.4 – 1.9 (6)
Stream <sup>a</sup>	Gas		0.12	0.10	0.5 (7)
	Stars		0.6	0.4	

<sup>a</sup> The Stream is defined as material at Magellanic Longitude less than -30. We have also accounted for the distance in our simulated stream in order to properly compare to the observed mass, which is computed modulo the distance squared.

Note. — (1) van der Marel et al. (2002) : The outermost data point lies at 9 kpc; (2) Brüns et al. (2005); (3) van der Marel et al. (2009) ; (4) Kim et al. (1998); (5) Stanimirović et al. (2004); (6) Harris & Zaritsky (2006); (7) Here we have accounted for the average distance to the simulated streams. The measured value is  $1.25 \times 10^8 (d/55\text{kpc})^2$  (Brüns et al. 2005) +  $2.0 \times 10^7 (d/120)^2$  (Nidever et al. 2010). The quoted simulated gas mass refers to the total mass, not just that of the neutral HI, whereas the observed values refer to HI gas only.

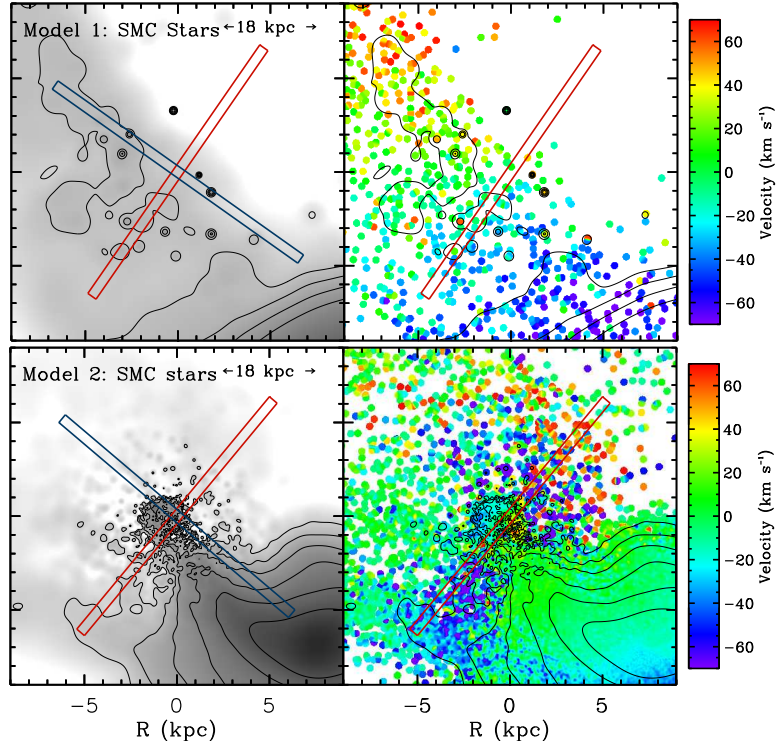


**Figure 19.** The kinematics of SMC stars that are captured by the LMC in Model 1 (top panel) and Model 2 (bottom panel) are illustrated in the line-of-sight frame of the LMC’s disk. Only particles initially belonging to the SMC are plotted. The center-of-mass velocity of the LMC’s stars has been subtracted from the velocity field of the transferred material. The left panels shows the stellar density map with the highest density contours overplotted. The size of each box is 11 kpc per side, the same as that in Figures 14 and 15 . The slit along the major and minor kinematic axes of the LMC are overplotted for reference. The color gradient ranging from blue to red indicates material moving towards (blue) and away (red) from the observer.

1998). Spiral structure “decays” along the sequence, with Sc having irregular spiral patterns and Im none at all. This is true also of the Barred Spiral sequence (SB), with asymmetry referring also to the appearance/location of the bar. Magellanic Irregulars encompass the late stages of both barred and unbarred spirals (e.g. Sd-Im, SBd-SBm); the LMC is classified as SBm under this scheme and the SMC an Im.

This work postulates that many barred Magellanic Irregulars may be perturbed versions of symmetric low-mass, bulgeless, barred galaxies, such as SBc type galaxies, where the bar is typically well-centered. We further illustrate a mode of inducing such perturbations, namely interactions with lower mass companions. In this picture, the LMC should not be thought of as a “dwarf” galaxy except in the sense that it is less luminous than the MW.

Asymmetric bars are typically not seen in massive galaxies, making them a defining characteristic of Magellanic Irregulars. This might be explained by noting that Sc/SBc type galaxies and Magellanic Irregulars (Sd-Im) are low mass systems compared to MW type galaxies and, correspondingly, they sample very different environments. Such galaxies do not have bulges, have shallower central potentials, are more dark matter dominated, have different halo concentration parameters, higher gas fractions and different ratios between the ISM temperature and virial temperature of their halos: all of these differences will influence the response of the system to tidal perturbations. As such, even if the physical scenario is similar (mass ratio and orbital configuration), the response of a MW type galaxy to a 1:10 mass ratio direct collision is expected to be different than an LMC-SMC ( $\sim 1:10$  mass ratio) encounter.

It is possible, for example, that the presence of a bulge may aid in stabilizing the bar of a high mass galaxy, preventing comparable asymmetries in the bar from arising. However, a detailed numerical study of such parameter space to test such conjectures is beyond the scope of the presented study.

Magellanic Irregulars are ubiquitous in our Local Volume. In light of the theory presented here, it must also be true that interactions between low-mass barred galaxies and smaller companions are a relatively frequent occurrence. From Hopkins et al. (2010), the expected galaxy major merger (mass ratio  $> 1/3$ ) rate is relatively flat as a function of host galaxy mass at  $z=0$ , so it is not expected that such encounters would be more likely for low mass systems. Stewart et al. (2008) find that 25-40% of hosts with mass of order  $\sim 10^{11} M_{\odot}/h$  have accreted a 1:10 mass ratio subhalo within the past 6-8 Gyr, which is the timescale for our isolated LMC-SMC interaction. This scenario is thus not at odds with cosmological expectations.

It has been pointed out by Wilcots & Prescott (2004) that many Magellanic Irregulars do not currently have companions, despite earlier claims of a high frequency of pairs by Odewahn (1994). However, the number of observed interacting dwarf systems is steadily increasing. Recently, Martinez-Delgado et al. (2011) have discovered a stellar stream about the Magellanic Irregular galaxy NGC 4449, which is an LMC analog in terms of its absolute magnitude. Although the stellar mass ratio of the disrupted object and the host is 1:50, the inferred dynamical mass ratio is between 1:10 - 1:5, making this system an analog of the late stages

of an LMC-SMC type tidal interaction. NGC 4449 was long thought to be an isolated Magellanic Irregular until observations of associated HI streams indicated that it likely had an encounter with an unseen companion (Hunter et al. 1998). Moreover, an unusual globular cluster exists in this galaxy with properties consistent with the nucleus of a disrupted galaxy (Annibali et al. 2011a,b); such observations indicate that the NGC 4449 may also have had more ancient accretion activity, which may partially explain the significant amount of mass in the HI streams surrounding the system. Signatures of earlier accretion events in dwarf galaxies has also been presented by Geha et al. (2005), who find evidence for a counterrotating core in the elliptical dwarf galaxy NGC 770 that they attribute to a minor merger event.

Such observations clearly illustrate that LMC mass objects do cannibalize smaller companions; however, the hallmarks of these encounters, such as faint tidal streams, are challenging to observe. The Wilcots & Prescott (2004) conclusions may thus indicate that the perturbing companion has already been cannibalized, causing most Magellanic Irregulars to appear as isolated objects. Moreover, the Mbaryon/Mtotal ratio is a steep function of mass for these low mass systems; many dwarfs in the local group have extremely large mass-to-light ratios. As such, a 1:10 total mass ratio companion may have a very discrepant stellar mass ratio, making the identification of such a companion challenging observationally.

In the context of the work presented here, Magellanic Irregulars are therefore key targets for deep HI and optical follow up observations as they are expected to be associated with tidal HI and stellar streams. Particular attention should be paid to Magellanic Irregulars with high current star formation rates, such as NGC 4449 and the LMC, which may point to ongoing tidal interactions with a low mass companion. Furthermore, there is clearly need for future observational and theoretical studies to better statistically quantify the frequency of interactions between LMC mass galaxies and smaller companions in order to assess the ubiquity of the theory presented here for the nature of Magellanic Irregulars.

## 6.6 Assessment of the Models

In this study we have explored the consequent large scale structure of the Magellanic System, the internal structure, kinematics of the LMC and the recent star formation histories of the MCs in a first infall scenario; i.e. without strong tidal torques from the MW. We focus on two different models for the interaction history of the LMC-SMC, one of which invokes a direct recent collision (Model 2), whereas in the other, the MCs never get closer than 20 kpc (Model 1). The ability of the presented models to reproduce key observed features of the Magellanic System are summarized in Table 5.

Both models are able to reproduce the global large scale structure of the Magellanic System. Overall, however, Model 1 provides better agreement with the properties of the Magellanic Stream, whereas Model 2 provides significantly better agreement with the structure and kinematics of the LMC.

While neither model reproduces every one of the features listed in Table 5 (and indeed the real answer is probably somewhere in between the two presented models) it is



**Table 5.** Observed Properties of the Magellanic System and How the Models Fare

Object	Property	Model 1	Model 2	Alternative
Large Scale Structure	A Leading Arm	Yes	Yes	
	Location of Leading Arm	No	No	Ram pressure
	A 150 degree Stream	Yes	Yes	
	Stream location offset from orbit	Yes	roughly	I.C. : SMC disk inclination
	Stream velocity gradient	Yes	roughly	I.C. : SMC disk inclination
	Stream bifurcation	roughly	No	Hydro instabilities
	Stream column gradient	No	No	Ram Pressure
				I.C. SMC gas mass
	Stream total mass	No	No	Ram Pressure;
				I.C. SMC gas mass
LMC	A Bridge	Yes	Yes	
	SF in Bridge	No	Yes	
	No SF in Stream	Yes	Yes	
	Rotation Curve	Yes	Yes	
	Offset gas and stellar kinematics	No	Yes	
	Offset bar	No	Yes	
	Bar not seen in gas	No	Yes	
	Warped stellar disk	Yes	Yes	
SMC	Elliptical stellar disk	roughly	Yes	
	Current SFR	No	No	SF details, feedback
	Increasing SFR < Gyr	No	Yes	
	Current SFR	No	No	SF details, feedback

Note. — SF stands for star formation. I.C. stand for initial conditions. The column marked Alternative indicates other possible factors that may help fix discrepancies between the observations and the models.

still rather remarkable that a single self-consistent model (namely Model 2) can simultaneously reproduce a large number of these features. Generally where the models fail (e.g. the column density gradient or location of the Leading Arm) the likely missing ingredients are ram pressure stripping owing to the passage of the galaxies through the ambient hot gaseous halo of the MW or a detailed search of model parameters (e.g. initial gas mass or orbital parameters). Inconsistencies with the current SFR and recent SFHs are almost certainly a result of the star formation prescriptions employed and the lack of stellar feedback.

A number of the discrepancies with the orbital model (e.g. the SMC's position and velocity) can likely be addressed by a complete parameter search of, e.g., plausible mass ratios between the two galaxies (we chose a fixed mass ratio of 1:10) and different orientations of the SMC disk relative to the LMC-SMC binary orbital plane. The inclination of the SMC's disk can dramatically alter the location and properties of the Stream, e.g. a retrograde coplanar configuration would inhibit the formation of a stream entirely. It can also change the way LMC torques affect the SMC's motion. This is likely the explanation for why the Model 2 results do not reproduce the exact velocity field or location of the Stream.

The Stream is also known to be both spatially and kinematically bifurcated, leading Putman et al. (2003) to describe it as a “twisted helix”. The Stream in our Model 1 is not of constant column density along its width; between Magellanic Longitudes of -50 and -100 the simulated stream appears to split into two high column density fila-

ments. This bifurcation is largely a result of the rotation of the SMC's initial disk. Note also that because the Stream is seen in projection, the appearance of this bifurcation is highly dependent on the viewing orientation (which is model dependent). This is likely why similar structures are not seen as clearly in Model 2. But it should be noted that in the Gadget simulations the ISM is smoothed by an effective equation of state, whereas in reality inhomogeneities should be present in the real ISM (e.g. molecular clouds). Stripping from a clumpier SMC ISM would lead to differences in the distribution of the stripped material. We further expect that hydrodynamic instabilities, which are not modeled here, would capitalize on any initial density inhomogeneities and augment this bifurcation. It is clear from the significant observed turbulence (Nigra et al. 2010) and the existence of head-tail structures in cloudlets within the Stream (Putman et al. 2003, 2011), that hydrodynamic instabilities are shaping its internal structure. Gas drag will operate differently on these clumps depending on their densities, naturally leading to a velocity bifurcation as well.

Although strong perturbations in the LMC disk are expected from a close encounter with a 1:10 mass ratio companion, without a large parameter study of impact parameters for the collision and mass ratios, it is unclear how generically these results can be applied to Magellanic Irregulars. A future study of these parameters will assess the robustness and longevity of the presented asymmetric structures (i.e. offset bars and one-armed spirals). In particular, it remains unclear as to whether a direct collision is always

required to produce such structures. Regardless, the existence of Magellanic Irregulars with close pairs connected by gaseous bridges is certainly suggestive of a link to a similar interaction history as that of the MCs.

It is worth pointing out that while it has been speculated that many of the features listed in Table 5 were directly related to interactions with the SMC, most of these links have never been illustrated by numerical simulations which self-consistently reproduce the global large scale features of the system. In this light, particular successes of the simulations presented in this work include the reproduction of a warped, off-centered bar that is neither detectable in the gaseous disk nor actively forming stars while simultaneously forming a Bridge, Leading Arm and trailing 150 degree long Stream. Furthermore, we have not yet discussed the remarkable agreement of the simulated SMC model with its observed structure and kinematics from this same Model 2. These results will be outlined in a subsequent paper.

## 7 CONCLUSIONS

We have explored two models for the possible interaction history of the LMC and SMC in an effort to simultaneously reproduce both the large scale gaseous distribution of the Magellanic System and the internal structure and morphology of the LMC. Here we summarize our findings for the Magellanic System and the implications for the study of Magellanic Irregular galaxies more generally.

### 7.1 Conclusions for the Magellanic System

The resulting kinematics and structure of the LMC strongly favor a scenario in which the MCs have recently (100-300 Myr) experienced a direct collision (our Model 2). Orbital models where the SMC never gets closer than 20 kpc to the LMC (e.g. Model 1) are able to reproduce the large scale structure of the Magellanic System, but poorly match the LMC's internal properties. In particular, without a direct collision with the SMC, the LMC would be better described as a normal, symmetric barred spiral galaxy. An upcoming paper will also illustrate that the observed internal kinematics and morphology of the SMC are also better described by this same collision model (Besla et al., in prep).

This study illustrates that, surprisingly, the LMC's disk can maintain a fairly smooth stellar velocity field despite a direct collision with the SMC and that such a scenario can explain a number of observed features of the LMC disk:

- (i) The gas and stellar kinematic centers of the LMC disk are coincident; however they are offset from the photometric center (Cole et al. 2005).
- (ii) The old stellar disk of the LMC is thick and warped. The warping at the edges may give it a flared appearance (Alves & Nelson 2000).
- (iii) The bar is warped relative to the LMC disk plane by ten degrees and is off-center relative to the dynamical center of the gaseous disk. While an offset bar in the LMC has been suggested by numerous authors as being the result of collisions with the SMC (e.g., Subramaniam & Subramanian 2009; Subramanian 2003; Bekki & Chiba 2007) this is the first time it has been modeled self-consistently.

(iv) The bar is not seen in the gas distribution (Kim et al. 1998) or as a site of on-going star formation, likely because the bar is warped out of the plane, inhibiting efficient gas funneling.

(v) Gaseous “arms” similar to those seen in HI maps of the LMC (Nidever et al. 2010, 2008) are stripped out of the LMC by the SMC in the direction of the Magellanic Bridge. This “arm” was formed during a violent collision and may have signatures in polarization maps of the LMC's magnetic field (Mao et al. in prep). This result also implies that there should be a metallicity gradient along the Bridge, increasing towards the LMC owing to contamination by LMC gas.

(vi) A one-armed spiral is induced in the LMC's disk and is a site of on-going star formation.

(vii) Stellar debris from the SMC is expected in the same field of view as the LMC disk. These stars will have differing kinematics signatures from the local LMC disk velocity field (Olsen et al. 2011) and may be the source of microlensing events towards the LMC (Besla et al. in prep). Such tidally stripped stars are not expected in a pure ram pressure stripping model for the Stream.

(viii) The gaseous Bridge that connects the two galaxies is the site of on-going star formation, where the SFR increases along its length towards the SMC.

(ix) The Leading Arm extends  $>70$  degrees ahead of the MCs and the Magellanic Stream extends 150 degrees behind them, reproducing the full extent of the Magellanic System. The Leading Arm is a younger structure than the Stream since it formed as a tidal tail during the SMC's most recent orbit about the LMC.

These listed properties are a direct consequence of interactions with the SMC, confirming the suspicions of de Vaucouleurs & Freeman (1972) that the LMC's peculiar morphology does not owe to interactions with the MW.

### 7.2 Implications for Magellanic Irregulars

There is potentially much to learn about Magellanic Irregular galaxies as a class by studying the Magellanic System in detail. In this work we have shown that the off-center bar and one-armed spiral arm of the LMC may be a product of close encounters with its smaller companion, the SMC. We conclude that interactions between a massive dwarf and a smaller companion, even one 10 times smaller in mass, can significantly alter the morphology of an otherwise normal looking, low-mass spiral galaxy. This study thus indicates that dwarf-dwarf galaxy interactions can be important drivers of their morphological evolution, without relying on interactions with a massive host.

Given that off-center bars and one-armed spirals are common characteristics of Magellanic Irregulars (de Vaucouleurs 1964), it is possible that such galaxies currently have or once had small companions. Known examples of Magellanic Irregulars with a close companion are thus prime candidates for follow up HI surveys to map the extended HI distribution, as the bridges that connect them likely have tidal tail counterparts. We argue here that if such systems were accreted by a massive spiral, they could form an analogous Magellanic System, i.e. two interacting dwarfs surrounded by an extended HI complex. A potential example could be the interacting pair of MC analogs,

NGC 4485/4490, which are surrounded by an extensive HI envelope but are not in close proximity to a massive host (Clemens et al. 1998). The recently identified stellar stream about the Magellanic Irregular galaxy NGC 4449 (Martinez-Delgado et al. 2011) gives further credence to this theory.

Quantifying the efficiency with which such dwarf-dwarf tidal interactions can remove gaseous material is directly relevant to questions about how dwarf galaxies lose their gas and how gas is supplied to more massive galaxies. The frequency of such dwarf-dwarf encounters has not yet been quantified observationally or theoretically. As such, the relative importance of such encounters remains to be determined. However, by reproducing the large scale structure of the Magellanic System in a LMC-SMC tidal scenario, we have shown here that at least 50% of the original gas budget of a small dwarf can be easily removed by tidal interactions with a larger dwarf companion, making such encounters a potentially important mode of baryon loss on these mass scales.

While the accretion of an LMC+SMC analog by a MW type host is a relatively rare event today (Boylan-Kolchin et al. 2011; Liu et al. 2011), modern models for the cosmological assembly of galactic-scale structures suggest that the MW halo formed from the earlier accretion and disruption of LMC-mass objects (Stewart et al. 2008). As such, simulations of isolated Magellanic Irregulars (LMC analogs) with low mass companions and the direct comparisons of such simulations to observed analogs, such as NGC 4027 (Phookun et al. 1992) and NGC 3664 (Wilcots & Prescott 2004), provides a logical testing ground for our understanding of the morphological, kinematic and chemical evolution of the fundamental building block of a MW-type galaxy.

## ACKNOWLEDGMENTS

The simulations in this paper were run on the Odyssey cluster supported by the FAS Science Division Research Computing Group at Harvard University. We thank Knut Olsen, Alar Toomre, David Nidever, Crystal Martin, Patrik Jonsson, Mary Putman and Dennis Zaritsky for useful discussions that have contributed to this paper. GB acknowledges support from NASA through Hubble Fellowship grant HST-HF-51284.01-A.

## APPENDIX A: THE ROLE OF RAM PRESSURE STRIPPING IN THE FORMATION OF THE STREAM

Evidence for the existence of a hot gaseous halo component of our MW comes from absorption lines towards distant AGN (Sembach et al. 2003). The MCs are therefore known to be moving through some ambient medium, and so the effects of ram pressure stripping and gas drag likely play some role in explaining the gas distribution of the Magellanic System. Our contention is that the impact of ram pressure is to modify the properties (velocity, location, mass) of the gas distribution, but does not in itself explain the existence of the Stream, Bridge and Leading Arm Feature.

To model the impact of ram pressure from a physical ambient medium representing the MW’s gaseous halo with either an SPH or Eulerian grid-based code would require extremely high numerical resolution, as the gaseous stream is very diffuse. Instead, we have created a toy simulation, where the Gadget-3 code was modified to include a ram pressure acceleration term that is applied uniformly to all gas particles and operates opposite to the direction of motion of those gas particles. Following the Gunn & Gott (1972) prescription, the ram pressure experienced by a gas particle moving through the hot gaseous halo of the MW (density,  $\rho_{\text{hot}}$ ), at a speed  $v_{\text{gal}}$  is expressed as follows:

$$P_{\text{ram}} = \rho_{\text{hot}} v_{\text{gal}}^2. \quad (\text{A1})$$

The acceleration experienced by a gas cloud of surface density  $\Sigma_{\text{gas}}$  owing to ram pressure is:

$$a_{\text{ram}} = P_{\text{ram}} / \Sigma_{\text{gas}}. \quad (\text{A2})$$

Following Vollmer et al. (2001), we can describe an HI gas cloud as having a characteristic column density of  $N_{\text{HI}} = 7.5 \times 10^{20} \text{ cm}^{-2}$  (Sanders et al. 1985). Thus,  $\Sigma_{\text{gas}} \sim N_{\text{HI}} \times m_{\text{HI}}$ . For a given velocity component  $v_{i=x,y,z}$ , the corresponding acceleration applied in that direction per timestep is:

$$\mathbf{a}_i = -\frac{n_{\text{hot}}}{N_{\text{HI}}} v_i^2 \frac{\mathbf{v}_i}{v}, \quad (\text{A3})$$

where the volume density ( $\rho_{\text{hot}}$ ) has been replaced by the number density of the MW’s ambient halo medium ( $n_{\text{hot}}$ ) multiplied by the mass of the average particle in the halo, which we have assumed is  $\sim m_{\text{HI}}$ . The quantity  $n_{\text{hot}}$  is largely unconstrained, although an upper limit of  $5 \times 10^{-4} \text{ cm}^{-3}$  is estimated (Rasmussen & Pedersen 2001; Maloney & Bland-Hawthorn 1999). We consider three values for this parameter:  $5 \times 10^{-5}$ ,  $10^{-4}$  and  $5 \times 10^{-4} \text{ cm}^{-3}$ . We further assume that this density is constant all the way to  $R_{200} = 220 \text{ kpc}$  of the MW. The ram pressure acceleration is applied to all gas particles as soon as the MCs enter within  $R_{200}$  of the MW. Note that this acceleration will not be constant as a function of time since the velocity of the particles changes as the MCs fall towards the MW.

We stress that this is a crude model, as there is no actual ambient gas density present and the force is applied uniformly to all particles. In reality, gas in the inner parts of the disk should be shielded by those on the outside. Moreover, other hydrodynamical instabilities, such as Kelvin-Helmoltz and Rayleigh-Taylor, will not be modeled in this set-up and we will therefore underestimate the amount of gas loss the galaxies may incur. This toy model will, however, give us a rough idea of how the position of the simulated Leading Arm, Bridge and Stream will evolve over time.

In Figure A1 and A2 the gas column density of the Magellanic System is mapped in Magellanic coordinates for Model 1 and Model 2, respectively. As the background density is increased, the location of the Stream changes, and the gas begins to trace the orbit. In Besla et al. (2007) it was shown that the location of the LMC past orbit deviates from the location of the Stream on the plane of the sky. This result was further shown to be insensitive to the MW model

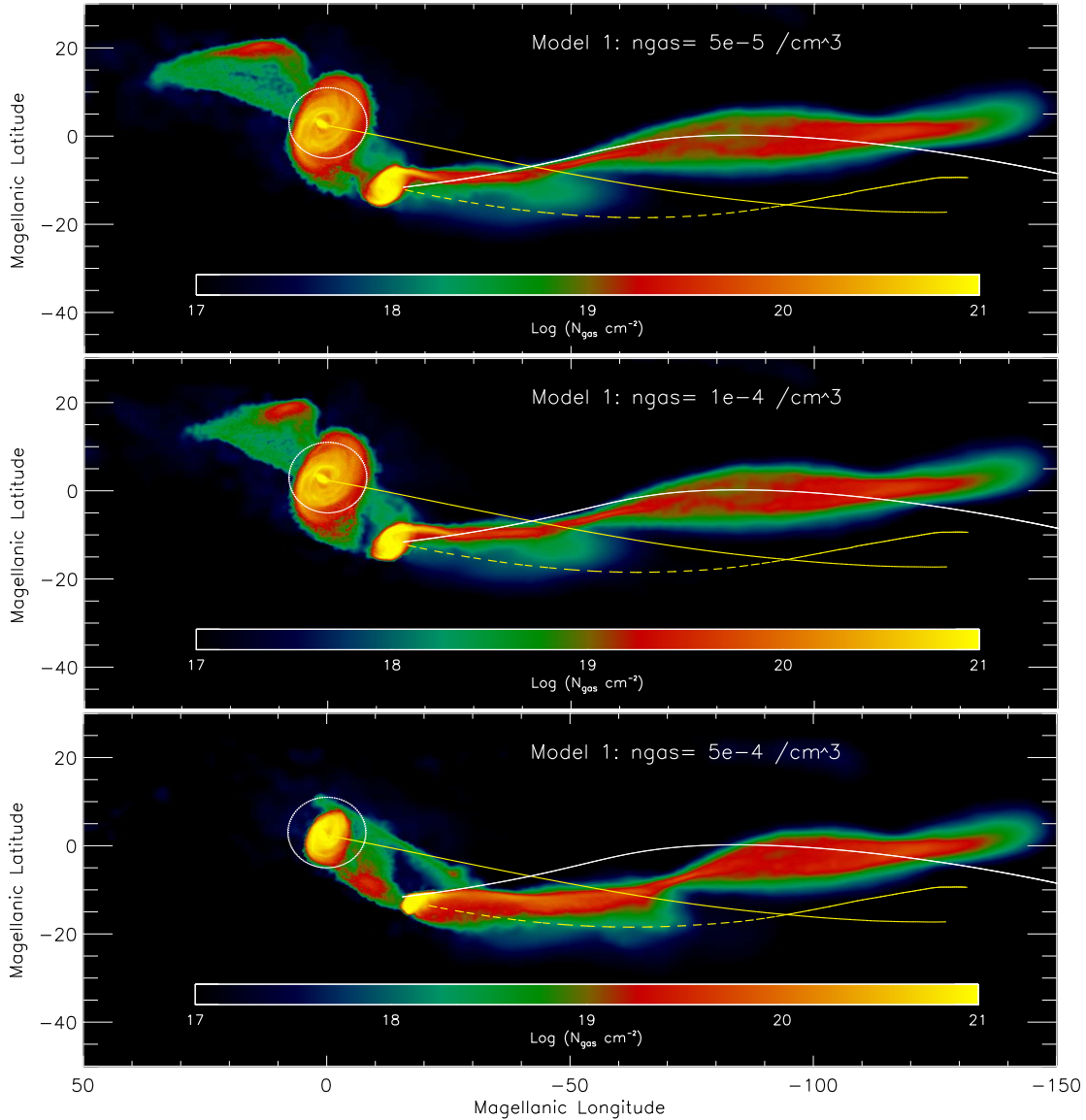


**Figure A1.** The gas column density in Magellanic Coordinates along the Magellanic System for Model 1 with a toy model ram pressure acceleration. The ambient hot halo gas density increases from top to bottom, as marked. Ram pressure causes the simulated stream to trace the past orbits of the Clouds on the plane of the sky; this is opposite to the location of the true Stream (indicated by the white line). The column density along the simulated stream also changes as the ram pressure becomes more important.

and robust within  $3\sigma$  of the measured proper motions. The fact that ram pressure stripping works to *align* the stripped material and the past orbits suggests that it is not the main formation mechanism for the Magellanic Stream.

The Leading Arm also changes location and structure significantly in the toy model, particularly in Model 1. Facing gas densities larger than  $10^{-4} \text{ cm}^{-3}$  it disappears entirely. Although the Bridge disappears in Model 1 at densities larger than  $5 \times 10^{-5} \text{ cm}^{-3}$ , it remains a strong feature in Model 2 at all densities. This is likely because, in Model 2, the Bridge is a young feature that formed in the most recent collision between the MCs. It has thus not had enough time to experience significant ram pressure effects. In Model 2 the leading arm also gets closer to the MW, falling to a line-of-sight distance of 30 kpc. These models do not predict that

components of the Leading Arm should be interacting with the gaseous disk of the MW, although there are claims that such a situation has been observed (McClure-Griffiths et al. 2008).

Note that as the ram pressure increases, the SMC's orbit changes; the SMC is clearly not in the same location in the lower panel of Figures A1 and A2 as in the respective upper panel. This occurs because ram pressure decreases the velocity of the SMC. The LMC, on the other hand, is too massive for its motion to be affected. A strong ram pressure headwind is thus likely at odds with the high relative velocity observed between the MCs ( $\sim 100 \text{ km/s}$ , Kallivayalil et al. 2006b).

The structure of the LMC gas disk changes even with a mild ram pressure headwind. The gas disk is rotating clock-

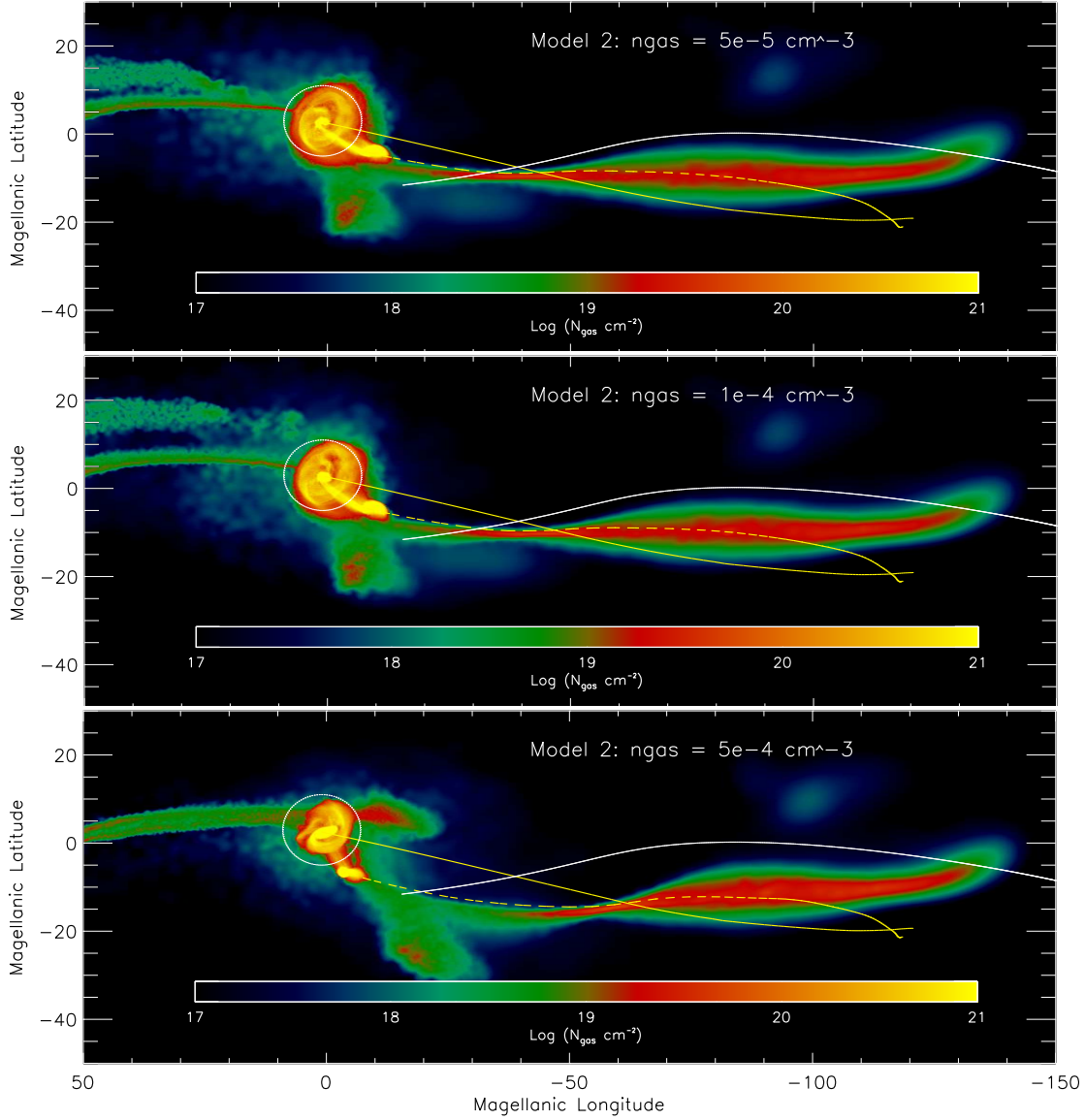


**Figure A2.** Same as Figure A1, but for Model 2.

wise, and so the lower half is rotating into the head wind and gets stalled. Gas therefore builds up in the lower left corner of the LMC's disk. This is in fact where the 30 Doradus star-forming region is situated. de Boer et al. (1998) suggested that the HI overdensity seen in the South-East is a direct result of the interaction between the rotating LMC gaseous disk and a headwind from the ambient medium. Here, we can indeed see that this process occurs generically in both Models 1 and 2. The LMC's gaseous disk is observed to be truncated (i.e. it is not as extended as the stellar disk). The simulated LMC gas disk is truncated if the ambient gas density is at least of order  $5 \times 10^{-5} \text{ cm}^{-3}$ .

Note that the column density along the Stream also changes as ram pressure become more important. The column density increases in the regions closest to the MCs, indicating that ram pressure may be the solution for the mismatch between the observed maximal column density

gradient along the Stream and the simulation results presented in Figure 8.

From this simple toy model we can conclude that ram pressure and other hydrodynamic instabilities will change the mass budget in the various components of the system and change their locations on the plane of the sky. In particular, ram pressure works to align the Stream with the past orbits, contrary to expectations from the proper motions (Besla et al. 2007). We estimate that if the background halo gas densities are in excess of  $10^{-4} \text{ /cm}^3$  the gas distribution of the simulated Magellanic System will be irreconcilable with observations. This estimate is in accord with observational upper limits (Rasmussen & Pedersen 2001).

A recent study by Diaz & Bekki (2011b) suggests that ram pressure at the ambient densities required by the Mastropietro et al. (2005) study ( $5 \times 10^{-5} \text{ /cm}^3$ ) would be too large for the survival of the Magellanic Stream. In a first infall scenario, where the Magellanic System would be inter-

acting with the ambient halo medium for a shorter period of time ( $< 1$  Gyr), we find that the Stream can indeed survive such densities and that ram pressure stripping likely plays a very important role in shaping the Magellanic Stream (particularly the Leading Arm) and increasing its mass budget. It should also be noted that Faraday rotation has been detected in at least one high velocity cloud in the Leading Arm (McClure-Griffiths et al. 2010); magnetic fields may protect the cloudlets from evaporation and hydrodynamic instabilities, increasing the chance of survivability of the Stream in the face of a ram pressure headwind.

## APPENDIX B: THE ROLE OF STELLAR FEEDBACK IN THE FORMATION OF THE STREAM

There is evidence of stellar feedback in the vicinity of the MCs. Lehner et al. (2009) have detected high velocity clouds (HVCs) between the MCs and the MW, moving at a velocity with respect to the local standard of rest ( $v_{lsr}$ ) as high as 150 km/s. Using FUSE, they find on average that these HVCs have metallicities of  $[OI/HI] = -0.51^{+0.12}_{-0.16}$  and HI masses of  $(0.5-1) \times 10^6 M_{\odot}$ , although these HVCs are predominantly ionized. Such material is thus, on average, enriched relative to the LMC and SMC. Furthermore, Lehner & Howk (2007) have detected a highly ionized (OVI, CIV, SiIV, NV) corona of high velocity gas surrounding the LMC, suggestive of outflows. Staveley-Smith et al. (2003b) also report similar observations, and find some of this high velocity gas to be projected on HI voids in the LMC. Data from FUSE indicates that the SMC appears to also have an OVI corona (Hoopes et al. 2002). These detected structures are in close proximity to the MCs, and so may be indicative of mass loss processes that are currently ongoing, rather than a long duration process that would be required to build the Magellanic Stream.

Recently, Nidever et al. (2008) found a coherent  $v_{lsr}$  gradient from the LMC along one of the filaments in the Stream and in the Leading Arm. They also claim to detect sinusoidal velocity patterns in the Stream, which they interpret as signatures of the LMC's disk rotation. They thus conclude that as much as half of the mass within the Stream originates from the LMC and that the sinusoidal velocity pattern indicates that the bulk of this material is emanating from the south-east HI overdensity (SEHO) region of the LMC's HI gaseous disk as a stellar outflow over the past 1.7 Gyr. The idea that the Magellanic Stream was formed from stellar outflows was also suggested by Olano (2004). The LMC is pock-marked with giant superbubbles, indicating locations of strong stellar feedback/winds. If the column density were constant across the disk, then each superbubble would have originally contained roughly  $10^7 M_{\odot}$  worth of material (Kim et al. 1998, 1999). Nidever et al. (2008) determine that 2-3 superbubbles losing  $10^6 M_{\odot}$  worth of material every 10 Myr over 1.7 Gyr would be sufficient to explain the mass budget of the Stream.

A stellar feedback model for the Stream is attractive in that it does not rely on strong MW tides to remove material from the LMC, making it consistent with a first infall scenario (although the leading component would still be an issue).

However, it is unlikely that outflows generated by SNe feedback would be sufficiently energetic to be unbound from the LMC's gravitational potential. In our first infall LMC models ( $M_{LMC} = 1.8 \times 10^{11} M_{\odot}$ ), the escape speed is of order 250 km/s at 10 kpc. Martin (2005) finds that terminal velocities expected from galaxies with maximum circular velocities of 100 km/s should also be of order 100 km/s, well below the escape speed at 10 kpc. Moreover, galaxies with star formation rates as low as  $0.1 M_{\odot}/\text{yr}$  (i.e. the value in the 30 Doradus region today, Harris & Zaritsky 2009) generally have outflow velocities less than 30 km/s (figure 6 of Martin 2005).

However, it is certainly possible that a ram pressure headwind can exploit the stellar feedback processes to aid in the removal of material from the deepest parts of the LMC's potential. This theory is testable by observations of the metallicity in the Stream: not only do the LMC and SMC have different metallicities, but any feedback scenario will result in the removal of enriched material (Mac Low & Ferrara 1999).

Metallicities for various components of the Magellanic System are summarized in Table B1. The current day LMC's metallicity is  $[O/H]_{LMC} = -0.34 \pm 0.06$  (Russell & Dopita 1992, updated to the latest solar abundances by Fox et al. 2010). But chemical enrichment models of Pagel & Tautvaisiene (1998) suggest that 2 Gyr ago the LMC's metallicity could have been as low as  $[O/H]_{LMC} \sim -0.5$  (their Figure 3). 1-2 Gyr is the relevant timescale for the formation of the Stream (Nidever et al. 2008; Gardiner & Noguchi 1996); given the measured  $H_{\alpha}$  emission along its length (Weiner & Williams 1996) and the corresponding expected ablation timescale for the neutral HI component of the Stream (Bland-Hawthorn et al. 2007), it is unlikely that the Stream could have survived for much longer.

Recently, Fox et al. (2010) have determined the oxygen abundance for a region near the tip of the Stream from absorption lines towards the background quasar NGC 7469. Observed  $[OI/HI]$  abundances are a close indication of the true oxygen abundance,  $[O/H]$ , since oxygen is not strongly depleted onto interstellar dust (Jensen et al. 2005). They find:

$$\left[\frac{O}{H}\right] \sim \left[\frac{OI}{HI}\right] = \log\left(\frac{N(OI)}{N(HI)}\right) - \log\left(\frac{O}{H}\right)_{\odot} \quad (B1)$$

$$= \log\left(\frac{10^{14.32 \pm 0.04}}{10^{18.63 \pm 0.13}}\right) - (-3.31) \quad (B2)$$

$$= -1.00 \pm 0.05(\text{stat}) \pm 0.08(\text{syst}) \quad (B3)$$

In an outflow or ram pressure stripping scenario the metallicity of the Stream must be at least that of the original ISM. These measurements make it improbable that the Stream could have solely originated in the LMC, regardless of the formation mechanism. The SMC interstellar oxygen abundance is a better match to these observations (see Table B1), especially since it was also less enriched 1-2 Gyr ago (Pagel & Tautvaisiene 1998). Interestingly, such low abundances are also measured in the Bridge connecting the MCs (Table B1; Lehner et al. 2008), suggestive of a common origin for both structures.

Closer to the MCs, the metallicity measurements de-

rived from absorption lines towards background quasars are larger by a factor of 2-4 (Lu et al. 1998; Gibson et al. 2000; Sembach et al. 2001). But these other measurements also have much larger error bars, as they use tracers that are more sensitive to ionization corrections than the OI/HI ratio. If we take an upper limit of a factor of 4 increase in the oxygen abundance in the Stream relative to the Fox et al. (2010) values, we can assess whether this material could have once ( $\sim 2$  Gyr ago) originated in a stellar wind from the LMC. We follow the methodology of Martin et al. (2002), who estimate the expected metallicity of outflows from the starbursting dwarf NGC 1569. The total mass of the ejected wind  $M_w$  is given by

$$M_w = M_{ej}(1 + \chi), \quad (\text{B4})$$

where  $M_{ej}$  is the mass in SNe ejecta and  $\chi$  is the mass loading of the wind. We consider first the required mass loading from the ISM of the LMC needed to dilute the metallicity so as to not violate the upper limits for the Stream. The oxygen abundance of the wind can be expressed as,

$$Z_{O,w} = \frac{M_{ej}(Z_{O,SN} + \chi Z_{O,ISM})}{M_w}. \quad (\text{B5})$$

Written in terms of the solar values, the abundance of the ISM 2 Gyr ago is  $Z_{O,ISM} = 10^{-0.5} = 0.32$ . Following Martin et al. (2002), the IMF-averaged metallicity of SNe ejecta is  $Z_{O,SN} \sim 8$  times solar for oxygen. We choose three values for  $Z_{O,SN} = 4, 8$  and  $12$ . We can rewrite equation B5 to solve for  $\chi$  in a mass independent way using equation B4:

$$\chi = \frac{Z_{O,SN} - Z_{O,w}}{Z_{O,w} - Z_{O,ISM}}. \quad (\text{B6})$$

Given that we know the current upper limit for the metallicity of the wind,  $Z_{O,w} = 10^{-0.4} = 0.4$ , then the required mass loading is  $\chi(Z_{O,SN} = 4, 8, 12) = (45, 95, 145)$ .

Mass loading in excess of factors of 10 are not observed. The wind from M82 is expected to be mass loaded by a factor of 3-6 (Suchkov et al. 1996) and Martin et al. (2002) find a value of  $\chi = 9$  to be favored for NGC 1569. Furthermore, numerical simulations by Mac Low & Ferrara (1999) find it difficult to accelerate any ambient cool gas that is swept up with the expanding outflow; instead, much of that material remains bound to the galaxy.

Ram pressure stripping might be the key missing ingredient that could help entrain ambient gas and explain such high mass loading factors. Assuming the addition of ram pressure stripping results in mass loading in excess of a factor of 45, then the resulting total wind mass (equation B4) over a timescale of 1.7 Gyr (the lifetime of the Stream according to the Nidever et al. 2008 model) would be of order  $M_w \sim 10^9 M_\odot^2$ . While this appears to be more than enough material to explain the total amount of neutral HI observed in the Stream ( $5 \times 10^8 M_\odot$ ; Table 4), it would imply that the entire Stream should be metal enriched, contrary to observations. This scenario thus over-predicts the mass budget of

the Stream and requires mass loading factors that are more extreme than observed.

## REFERENCES

- Agertz O. et al., 2007, MNRAS, 380, 963  
 Alves D. R., Nelson C. A., 2000, ApJ, 542, 789  
 Annibali F., Tosi M., Aloisi A., van der Marel R. P., 2011a, AJ, 142, 129  
 Annibali F., Tosi M., Aloisi A., van der Marel R. P., Martinez-Delgado D., 2011b, ArXiv e-prints  
 Bauer A., Springel V., 2011, ArXiv e-prints  
 Bekki K., 2009, MNRAS, 393, L60  
 Bekki K., Chiba M., 2005, MNRAS, 356, 680  
 Bekki K., Chiba M., 2007, Publications of the Astronomical Society of Australia, 24, 21  
 Besla G., Kallivayalil N., Hernquist L., Robertson B., Cox T. J., van der Marel R. P., Alcock C., 2007, ApJ, 668, 949  
 Besla G., Kallivayalil N., Hernquist L., van der Marel R. P., Cox T. J., Kereš D., 2010, ApJ, 721, L97, [B10]  
 Binney J., Fraternali F., 2011, ArXiv e-prints  
 Binney J., Merrifield M., 1998, Galactic Astronomy, Binney, J. & Merrifield, M., ed.  
 Bland-Hawthorn J., Sutherland R., Agertz O., Moore B., 2007, ApJ, 670, L109  
 Book L. G., Chu Y.-H., Gruendl R. A., 2008, ApJS, 175, 165  
 Book L. G., Chu Y.-H., Gruendl R. A., Fukui Y., 2009, AJ, 137, 3599  
 Boylan-Kolchin M., Besla G., Hernquist L., 2011, MNRAS, 414, 1560  
 Brüns C. et al., 2005, A&A, 432, 45  
 Busha M. T., Marshall P. J., Wechsler R. H., Klypin A., Primack J., 2011, ApJ, 743, 40  
 Choi J.-H., Weinberg M. D., Katz N., 2007, MNRAS, 381, 987  
 Clemens M. S., Alexander P., Green D. A., 1998, MNRAS, 297, 1015  
 Cole A. A., Tolstoy E., Gallagher, III J. S., Smecker-Hane T. A., 2005, AJ, 129, 1465  
 Connors T. W., Kawata D., Gibson B. K., 2005, ArXiv Astrophysics e-prints  
 Connors T. W., Kawata D., Gibson B. K., 2006, MNRAS, 371, 108  
 de Boer K. S., Braun J. M., Vallenari A., Mebold U., 1998, A&A, 329, L49  
 de Vaucouleurs G., 1964, in IAU Symposium, Vol. 20, The Galaxy and the Magellanic Clouds, F. J. Kerr, ed., pp. 269–+  
 de Vaucouleurs G., Freeman K. C., 1972, Vistas in Astronomy, 14, 163  
 Demers S., Battinelli P., 1998, AJ, 115, 154  
 Diaz J., Bekki K., 2011a, MNRAS, 413, 2015  
 Diaz J., Bekki K., 2011b, Publications of the Astronomical Society of Australia, 28, 117  
 D’Onghia E., Besla G., Cox T. J., Hernquist L., 2009, Nature, 460, 605  
 D’Onghia E., Lake G., 2008, ApJ, 686, L61  
 D’Onghia E., Vogelsberger M., Faucher-Giguere C.-A., Hernquist L., 2010, ApJ, 725, 353

<sup>2</sup>  $M_{ej} = \Gamma \dot{M}_* T_{MS}$  is determined assuming a star formation rate of  $\dot{M}_* = 0.1 M_\odot/\text{yr}$  (the current rate in 30 Doradus), a SNe formation rate of  $\Gamma = 0.12$  determined from Starburst99 (Leitherer et al. 1999) with a Kroupa IMF, over a timescale of  $T_{MS} = 1.7$  Gyr

**Table B1.** Oxygen Abundances

Object	[O/H] <sup>a</sup>	Reference
LMC (today)	-0.34 ± 0.6	Russell & Dopita (1992); Fox et al. (2010)
LMC (2 Gyr ago)	-0.5	Pagel & Tautvaisiene (1998)
SMC (today)	-0.66 ± 0.1	Russell & Dopita (1992); Fox et al. (2010)
Stream	-1.0 ± 0.13	Fox et al. (2010)
Stream (Upper Limit) <sup>b</sup>	-0.4	Gibson et al. (2000); Lu et al. (1998); Sembach et al. (2001)
Bridge	-0.96 <sup>+0.13</sup> <sub>-0.11</sub>	Lehner et al. (2008)
HVCs near LMC	-0.5 <sup>+0.12</sup> <sub>-0.16</sub>	Lehner et al. (2009)

<sup>a</sup> Log of the oxygen abundance relative to solar, as defined in equation B2.

<sup>b</sup> Upper limit is defined by increasing the observed oxygen column density of the Stream by a factor of four

- Fox A. J., Wakker B. P., Smoker J. V., Richter P., Savage B. D., Sembach K. R., 2010, *ApJ*, 718, 1046
- Freedman Woods D., Geller M. J., Kurtz M. J., Westra E., Fabricant D. G., Dell'Antonio I., 2010, *AJ*, 139, 1857
- Gardiner L. T., Noguchi M., 1996, *MNRAS*, 278, 191, [GN96]
- Gardiner L. T., Sawa T., Fujimoto M., 1994, *MNRAS*, 266, 567, [GSF94]
- Geha M., Blanton M. R., Masjedi M., West A. A., 2006, *ApJ*, 653, 240
- Geha M., Guhathakurta P., van der Marel R. P., 2005, *AJ*, 129, 2617
- Gibson B. K., Giroux M. L., Penton S. V., Putman M. E., Stocke J. T., Shull J. M., 2000, *AJ*, 120, 1830
- Gnedin N. Y., Kravtsov A. V., 2010, *ApJ*, 714, 287
- Gordon K. D. et al., 2009, *ApJ*, 690, L76
- Graff D. S., Gould A. P., Suntzeff N. B., Schommer R. A., Hardy E., 2000, *ApJ*, 540, 211
- Grcevich J., Putman M. E., 2009, *ApJ*, 696, 385
- Guhathakurta P., Reitzel D. B., 1998, in *ASP Conf. Ser.* 136: Galactic Halos, Zaritsky D., ed., p. 22
- Gunn J. E., Gott J. R. I., 1972, *ApJ*, 176, 1
- Guo Q., White S., Li C., Boylan-Kolchin M., 2010, *MNRAS*, 404, 1111
- Harris J., 2007, *ApJ*, 658, 345
- Harris J., Zaritsky D., 2006, *AJ*, 131, 2514
- Harris J., Zaritsky D., 2009, *AJ*, 138, 1243
- Heller P., Rohlfs K., 1994, *A&A*, 291, 743
- Hernquist L., 1990, *ApJ*, 356, 359
- Hoopes C. G., Sembach K. R., Howk J. C., Savage B. D., Fullerton A. W., 2002, *ApJ*, 569, 233
- Hopkins P. F., Cox T. J., Younger J. D., Hernquist L., 2009, *ApJ*, 691, 1168
- Hopkins P. F. et al., 2010, *ApJ*, 724, 915
- Hopkins P. F., Hernquist L., Cox T. J., Younger J. D., Besla G., 2008, *ApJ*, 688, 757
- Hopkins P. F., Quataert E., Murray N., 2011, *ArXiv e-prints*
- Hunter D. A., Wilcots E. M., van Woerden H., Gallagher J. S., Kohle S., 1998, *ApJ*, 495, L47
- James P. A., Ivory C. F., 2011, *MNRAS*, 411, 495
- Jensen A. G., Rachford B. L., Snow T. P., 2005, *ApJ*, 619, 891
- Jin S., Lynden-Bell D., 2008, *MNRAS*, 383, 1686
- Kallivayalil N., van der Marel R. P., Alcock C., 2006b, *ApJ*, 652, 1213, [K2]
- Kallivayalil N., van der Marel R. P., Alcock C., Axelrod T., Cook K. H., Drake A. J., Geha M., 2006a, *ApJ*, 638, 772, [K1]
- Kennicutt, Jr. R. C., Hodge P. W., 1986, *ApJ*, 306, 130
- Keres D., Vogelsberger M., Sijacki D., Springel V., Hernquist L., 2011, *ArXiv e-prints*
- Kerr F. J., 1957, *AJ*, 62, 93
- Kim S., Dopita M. A., Staveley-Smith L., Bessell M. S., 1999, *AJ*, 118, 2797
- Kim S., Staveley-Smith L., Dopita M. A., Freeman K. C., Sault R. J., Kesteven M. J., McConnell D., 1998, *ApJ*, 503, 674
- Koerwer J. F., 2009, *AJ*, 138, 1
- Kreckel K. et al., 2011, *AJ*, 141, 4
- Krumholz M. R., McKee C. F., Tumlinson J., 2009, *ApJ*, 699, 850
- Kuhlen M., Krumholz M., Madau P., Smith B., Wise J., 2011, *ArXiv e-prints*
- Lah P., Kiss L. L., Bedding T. R., 2005, *MNRAS*, 359, L42
- Larson R. B., Tinsley B. M., 1978, *ApJ*, 219, 46
- Lehner N., Howk J. C., 2007, *MNRAS*, 377, 687
- Lehner N., Howk J. C., Keenan F. P., Smoker J. V., 2008, *ApJ*, 678, 219
- Lehner N., Staveley-Smith L., Howk J. C., 2009, *ApJ*, 702, 940
- Leitherer C. et al., 1999, *ApJS*, 123, 3
- Levine S. E., Sparke L. S., 1998, *ApJ*, 496, L13
- Lin D. N. C., Jones B. F., Klemola A. R., 1995, *ApJ*, 439, 652
- Liu L., Gerke B. F., Wechsler R. H., Behroozi P. S., Busha M. T., 2011, *ApJ*, 733, 62
- Lu L., Sargent W. L. W., Savage B. D., Wakker B. P., Sembach K. R., Oosterloo T. A., 1998, *AJ*, 115, 162
- Lynds R., Toomre A., 1976, *ApJ*, 209, 382
- Mac Low M.-M., Ferrara A., 1999, *ApJ*, 513, 142
- Maloney P. R., Bland-Hawthorn J., 1999, *ApJ*, 522, L81
- Martin C. L., 2005, *ApJ*, 621, 227
- Martin C. L., Kobulnicky H. A., Heckman T. M., 2002, *ApJ*, 574, 663
- Martinez-Delgado D. et al., 2011, *ArXiv e-prints*
- Mastropietro C., Burkert A., Moore B., 2009, *MNRAS*, 399, 2004
- Mastropietro C., Moore B., Mayer L., Wadsley J., Stadel J., 2005, *MNRAS*, 363, 509



- Mathewson D. S., Cleary M. N., Murray J. D., 1974, *ApJ*, 190, 291
- Matthews D., Staveley-Smith L., Dyson P., Muller E., 2009, *ApJ*, 691, L115
- McClure-Griffiths N. M., Madsen G. J., Gaensler B. M., McConnell D., Schnitzeler D. H. F. M., 2010, *ApJ*, 725, 275
- McClure-Griffiths N. M. et al., 2008, *ApJ*, 673, L143
- McCumber M. P., Garnett D. R., Dufour R. J., 2005, *AJ*, 130, 1083
- Mellinger A., 2009, *PASP*, 121, 1180
- Moore B., Davis M., 1994, *MNRAS*, 270, 209
- Murai T., Fujimoto M., 1980, *PASJ*, 32, 581
- Murray N., Rahman M., 2010, *ApJ*, 709, 424
- Navarro J. F., Frenk C. S., White S. D. M., 1997, *ApJ*, 490, 493
- Nidever D. L., Majewski S. R., Burton W. B., 2008, *ApJ*, 679, 432
- Nidever D. L., Majewski S. R., Butler Burton W., Nigra L., 2010, *ApJ*, 723, 1618
- Nigra L., Stanimirovic S., Gallagher, III J. S., Lockman F. J., Nidever D. L., Majewski S. R., 2010, in *Astronomical Society of the Pacific Conference Series*, Vol. 423, *Galaxy Wars: Stellar Populations and Star Formation in Interacting Galaxies*, B. Smith, J. Higdon, S. Higdon, & N. Bastian, ed., pp. 38–+
- Nikolaev S., Drake A. J., Keller S. C., Cook K. H., Dalal N., Griest K., Welch D. L., Kanbur S. M., 2004, *ApJ*, 601, 260
- Noël N. E. D., Aparicio A., Gallart C., Hidalgo S. L., Costa E., Méndez R. A., 2009, *ApJ*, 705, 1260
- Odewahn S. C., 1994, *AJ*, 107, 1320
- Olano C. A., 2004, *A&A*, 423, 895
- Olsen K. A. G., Massey P., 2007, *ArXiv Astrophysics e-prints*
- Olsen K. A. G., Salyk C., 2002, *AJ*, 124, 2045
- Olsen K. A. G., Zaritsky D., Blum R. D., Boyer M. L., Gordon K. D., 2011, *ArXiv e-prints*
- Padoan P., Kim S., Goodman A., Staveley-Smith L., 2001, *ApJ*, 555, L33
- Pagel B. E. J., Tautvaisiene G., 1998, *MNRAS*, 299, 535
- Patton D. R., Ellison S. L., Simard L., McConnell A. W., Mendel J. T., 2011, *MNRAS*, 412, 591
- Phookun B., Mundy L. G., Teuben P. J., Wainscoat R. J., 1992, *ApJ*, 400, 516
- Piatek S., Pryor C., Olszewski E. W., 2008, *AJ*, 135, 1024
- Pietrzynski G., Udalski A., 2000a, *Acta Astronomica*, 50, 337
- Pietrzynski G., Udalski A., 2000b, *Acta Astronomica*, 50, 355
- Putman M. E., Saul D. R., Mets E., 2011, *MNRAS*, 418, 1575
- Putman M. E., Staveley-Smith L., Freeman K. C., Gibson B. K., Barnes D. G., 2003, *ApJ*, 586, 170
- Rasmussen J., Pedersen K., 2001, *ApJ*, 559, 892
- Robertson B. E., Kravtsov A. V., 2008, *ApJ*, 680, 1083
- Russell S. C., Dopita M. A., 1992, *ApJ*, 384, 508
- Ružička A., Theis C., Palouš J., 2009, *ApJ*, 691, 1807
- Ružička A., Theis C., Palouš J., 2010, *ApJ*, 725, 369
- Sales L. V., Navarro J. F., Abadi M. G., Steinmetz M., 2007, *MNRAS*, 379, 1475
- Sanders D. B., Scoville N. Z., Solomon P. M., 1985, *ApJ*, 289, 373
- Sembach K. R., Howk J. C., Savage B. D., Shull J. M., 2001, *AJ*, 121, 992
- Sembach K. R. et al., 2003, *ApJS*, 146, 165
- Sijacki D., Vogelsberger M., Keres D., Springel V., Hernquist L., 2011, *ArXiv e-prints*
- Springel V., 2005, *MNRAS*, 364, 1105
- Springel V., 2010, *MNRAS*, 401, 791
- Springel V., Di Matteo T., Hernquist L., 2005, *MNRAS*, 361, 776
- Springel V., Hernquist L., 2002, *MNRAS*, 333, 649
- Springel V., Hernquist L., 2003, *MNRAS*, 339, 289
- Stanimirović S., Staveley-Smith L., Jones P. A., 2004, *ApJ*, 604, 176
- Staveley-Smith L., Kim S., Calabretta M. R., Haynes R. F., Kesteven M. J., 2003a, *MNRAS*, 339, 87
- Staveley-Smith L., Kim S., Calabretta M. R., Haynes R. F., Kesteven M. J., 2003b, *MNRAS*, 339, 87
- Stewart K. R., Bullock J. S., Wechsler R. H., Maller A. H., Zentner A. R., 2008, *ApJ*, 683, 597
- Struck C., 1997, *ApJS*, 113, 269
- Subramaniam A., 2003, *ApJ*, 598, L19
- Subramaniam A., Subramanian S., 2009, *ApJ*, 703, L37
- Suchkov A. A., Berman V. G., Heckman T. M., Balsara D. S., 1996, *ApJ*, 463, 528
- Swaters R. A., van Albada T. S., van der Hulst J. M., Sancisi R., 2002, *A&A*, 390, 829
- Tollerud E. J., Boylan-Kolchin M., Barton E. J., Bullock J. S., Trinh C. Q., 2011, *ApJ*, 738, 102
- Toomre A., Toomre J., 1972, *ApJ*, 178, 623
- Torrey P., Vogelsberger M., Sijacki D., Springel V., Hernquist L., 2011, *ArXiv e-prints*
- van den Bergh S., 2006, *AJ*, 132, 1571
- van der Marel R. P., 2001, *AJ*, 122, 1827
- van der Marel R. P., Alves D. R., Hardy E., Suntzeff N. B., 2002, *AJ*, 124, 2639, [vdM02]
- van der Marel R. P., Cioni M.-R. L., 2001, *AJ*, 122, 1807
- van der Marel R. P., Kallivayalil N., Besla G., 2009, in *IAU Symposium*, Vol. 256, *IAU Symposium*, J. T. van Loon & J. M. Oliveira, ed., pp. 81–92
- Vieira K. et al., 2010, *AJ*, 140, 1934, [V10]
- Vogelsberger M., Sijacki D., Keres D., Springel V., Hernquist L., 2011, *ArXiv e-prints*
- Vollmer B., Cayatte V., Balkowski C., Duschl W. J., 2001, *ApJ*, 561, 708
- Wannier P., Wrixon G. T., 1972, *ApJ*, 173, L119+
- Weil M. L., Hernquist L., 1993, *ApJ*, 405, 142
- Weiner B. J., Williams T. B., 1996, *AJ*, 111, 1156
- Whitney B. A. et al., 2008, *AJ*, 136, 18
- Wilcots E. M., 2009, in *IAU Symposium*, Vol. 256, *IAU Symposium*, J. T. van Loon & J. M. Oliveira, ed., pp. 461–472
- Wilcots E. M., Lehman C., Miller B., 1996, *AJ*, 111, 1575
- Wilcots E. M., Prescott M. K. M., 2004, *AJ*, 127, 1900
- Wilke K., Klaas U., Lemke D., Mattila K., Stickel M., Haas M., 2004, *A&A*, 414, 69
- Yoshizawa A. M., Noguchi M., 2003, *MNRAS*, 339, 1135
- Zaritsky D., 2004, *ApJ*, 614, L37
- Zaritsky D., Harris J., Grebel E. K., Thompson I. B., 2000, *ApJ*, 534, L53
- Zhao H., Evans N. W., 2000, *ApJ*, 545, L35